Industrial Crops & Products 240 (2026) 122708

Contents lists available at ScienceDirect

Industrial Crops & Products

journal homepage: www.elsevier.com/locate/indcrop

Polygonatum cyrtonema Hua endophytic bacterium *Bacillus amyloliquefaciens* HJ9 and its degenerate strain dHJ9: Antifungal activity and mechanisms

Xin-Pei Ye [a,1], Zi-Xin Wang [a,1], Yue Fu [a], Zhen-Xing Tang [b], Yan-Xi Chen [a], Shu-Qi Chen [a], Yu-Hang Zhou [a], Shu-Jie Lin [a], Yu-Huan Wu [a,c,*], Er-Xu Pi [a,c,*], Lu-E. Shi [a,c,*]

[a] Department of Biotechnology, College of Life and Environmental Sciences, Hangzhou Normal University, Hangzhou, Zhejiang 311121, PR China
[b] School of Hospitality Management and Culinary Arts, Tourism College of Zhejiang, Hangzhou, Zhejiang 311231, PR China
[c] Zhejiang Provincial Modern Biology and Medicine Industry College , Hangzhou Normal University, Hangzhou, Zhejiang, China

ARTICLE INFO

Keywords:
Bacillus amyloliquefaciens
Fusarium sp.
Antifungal activity
Mechanism
Degeneration

ABSTRACT

To control *Fusarium*-induced root rot in *Polygonatum cyrtonema* Hua, the endophytic antagonistic bacterium against root rot was screened in this work. Furthermore, antifungal capacity and mechanisms of the obtained *Bacillus amyloliquefaciens* (*B. amyloliquefaciens*) HJ9 and its degenerate strain dHJ9 were investigated. The obtained data demonstrated that cell-free supernatant (CFS) of *B. amyloliquefaciens* HJ9 significantly inhibited mycelial growth, spore germination, and biofilm formation of *Fusarium* sp. F2, whereas CFS of *B. amyloliquefaciens* dHJ9 exhibited substantially diminished antagonistic activity. The antifungal mechanism studies indicated that *B. amyloliquefaciens* HJ9 primarily disrupted the cell membrane integrity of *Fusarium* sp. F2, evidenced by increased membrane damage indicators. Pot trials confirmed that *B. amyloliquefaciens* HJ9 CFS showed optimal root rot control, superior to bacterial suspensions, whereas *B. amyloliquefaciens* dHJ9 treatment even exacerbated the disease. The degeneration resulted not only in the lose of key biosynthetic gene clusters, but also in a pronounced reduction in the production of the plant growth substances like indole-3-acetic acid (IAA). This study established a foundation for developing biocontrol agents based on the bioactive metabolites of endophytes from *P. cyrtonema* Hua.

1. Introduction

Polygonatum cyrtonema (*P. cyrtonema*) Hua, a perennial herb with both medicinal and food uses in the genus *Polygonatum*, plays an important role in Chinese traditional medical system (Liu et al., 2023b, 2024). Its rhizome accumulates various biological active ingredients, such as polysaccharides, saponins, flavonoids, alkaloids, etc (Huang et al., 2021; Han et al., 2023; Liu et al., 2023a; Shi et al., 2025). Recent pharmacological investigations have indicated that *P. cyrtonema* Hua exhibits a wide range of bioactivities, including antioxidant, anti-inflammatory, immunomodulatory, anti-tumor, and antibacterial activity, as well as the capacity to regulate metabolic disorders (Khan et al., 2012; Long et al., 2018; Zeng et al., 2020; He et al., 2022; Xu et al., 2023a; Yang et al., 2023). However, root rot caused by *Fusarium* spp. is one of the most devastating diseases limiting the sustainable cultivation of *P. cyrtonema* Hua (Lu et al., 2021; Pang et al., 2022; Wang et al., 2025b). Currently, chemical fungicides (*e.g.* carbendazim, mancozeb, thiabendazole) serve as the primary means of controlling *Fusarium*-induced diseases. However, their long-term and intensive use can lead to numerous concerns, including pathogen resistance, drug residues, and environmental pollution (Kaye et al., 2015; Liu et al., 2019; Gonzalez et al., 2020; Acosta-González et al., 2022; Yi et al., 2023; Mohan et al., 2024). Therefore, the development of green and efficient biocontrol strategies has become an urgent need for the sustainable cultivation of *P. cyrtonema* Hua.

Biological control has emerged as a highly promising alternative for controlling *Fusarium*-induced diseases, and has attracted increasing research interest in recent years (Aydin, 2019; Sharma et al., 2022). This approach utilizes beneficial microorganisms and/or their metabolites, offering advantages such as high water solubility, and strong antimicrobial properties (Ma et al., 2023). Unfortunately, many microorganisms, particularly those represented by *Bacillus* spp., are prone to

* Corresponding authors at: Department of Biotechnology, College of Life and Environmental Sciences, Hangzhou Normal University, Hangzhou, Zhejiang 311121, PR China.
E-mail addresses: yuhuanwu@hznu.edu.cn (Y.-H. Wu), erxupi@hznu.edu.cn (E.-X. Pi), shilue@hznu.edu.cn (L.-E. Shi).
[1] Xin-Pei Ye and Zi-Xin Wang contributed equally to this study and should be regarded as co-first author.

https://doi.org/10.1016/j.indcrop.2026.122708
Received 18 October 2025; Received in revised form 14 December 2025; Accepted 13 January 2026
Available online 20 January 2026

degeneration during serial subculturing, leading to a significant decline in their antagonistic activity and consequently restricting their practical application (Tang et al., 1996; Zhu and Yang, 2000; Ren et al., 2017). Kadam et al. (1987) indicated that the recombinant plasmid pEAA harboring the amylase gene in *B. subtilis* exhibited structural instability, frequently undergoing spontaneous deletion of the exogenous gene fragment to form the degenerate strain pEAA1, which led to the complete loss of amylase production ability. Similarly, in the study of Ren et al. (2017), the authors found that the high-yielding adenosine *B. subtilis* D14–24 degenerated primarily through high-frequency reversion mutations in its histidine auxotrophy (His^-), causing a decline in adenosine yield from 15.69 to 5.87 g/L. The degenerate isolate also displayed phenotypic abnormalities characterized by the aberrant accumulation of red-pigments metabolites (Ren et al., 2017). Therefore, strain degeneration remains a primary limitation for the utilization of biocontrol agents (Kadam et al., 1987).

Throughout their long-term co-evolution with plants, endophytic microorganisms have developed the ability to enhance host health by producing antimicrobial substances and inducing plant resistance, thereby suppressing pathogenic infections (Negi et al., 2024). In recent years, various studies have confirmed endophytes as valuable sources of biocontrol agents, contributing significantly to sustainable agriculture by reducing reliance on chemical pesticides and enhancing crop disease resistance (Chaudhary et al., 2022; Pandey et al., 2022). Endophytes have demonstrated efficacy in controlling root rot in various crops, such as wheat, sunflower, tomato, *Ligusticum chuanxiong* Hort, *Panax notoginseng* (Wang et al., 2023b; Chen et al., 2024; Li et al., 2024; Bui et al., 2025;.Urooj and Farhat, 2025). At present, several endophytes from with anti-microorganism activity have been isolated from *Polygonatum* species. Chi et al. (2019) isolated 11 strains of endophytes from the rhizomes, leaves, and stems of *P. cyrtonema* Hua, among which *B.velezensis* ZJU-3 exhibited strong antagonistic activity against *Fusarium oxysporum* (*F. oxysporum*). Zhai et al. (2019) isolated an endophytic bacterium, identified as *B. subtilis* HJ-2, from the rhizomes of *P. cyrtonema* Hua cultivated in Anhui province, China, whose fermentation broth demonstrated broad-spectrum antibacterial activity against *Escherichia coli* (*E. coli*), *Staphylococcus aureus* (*S. aureus*), and *Pseudomonas aeruginosa* (*P. aeruginosa*). However, the potential of endophytes in biocontrol against *Polygonatum* root rot remains unexplored. Moreover, like many other microorganisms, plant endophytes are highly susceptible to strain degeneration. The degeneration process often involves various functional losses, including diminished synthesis of antimicrobial secondary metabolites (*e.g.*, lipopeptides) and reduced production of plant growth-promoting substances like IAA. These changes compromise the efficacy and reliability of biocontrol agents, presenting a significant challenge to their industrial application. Therefore, to develop biocontrol strategies against *P. cyrtonema* Hua root rot, ~~i~~n this study, we isolated endophytic strains from healthy rhizomes and screened them for antagonistic activity against common pathogens. Furthermore, the antagonistic capacity and mechanisms of the selected endophyte and its degenerated variant were investigated. Specially, effect of the degeneration on plant growth-promoting traits (IAA production) was also evaluated. This study not only evaluated the biocontrol potential of the obtained endophytes, but also provided critical insights into the functional and genetic markers of strain stability. These findings would facilitate the practical application of sustainable biocontrol technology in managing *Fusarium*-induced root rot in *Polygonatum* species and other valuable medicinal crops.

2. Materials and methods

2.1. Isolation of endophytes with antibacterial activity from P. cyrtonema Hua

P. cyrtonema Hua were collected from Pan'an, Zhejiang Province, China in July 2024. Endophytes from *P. cyrtonema* Hua were isolated using the tissue separation method (Mao et al., 2021; Sahu et al., 2022). Fresh and healthy *P. cyrtonema* Hua were selected. Surface soil of the rhizomes was washed off. The rhizomes were then soaked in 75 % alcohol for 5 min. After that, the samples were soaked in 2.0 % sodium hypochlorite for 5 min. After surface sterilization, the rhizomes were aseptically cut into approximately 1 cm × 1 cm slices, and divided into two batches. One batch was inoculated onto LB agar media plates (tryptone 10.0 g/L, yeast extract 5.0 g/L, sodium chloride 10.0 g/L, agar 15.0 g/L), and incubated at 37 ℃ for 1–2 d, while the other batch was inoculated onto PDA plates (potato infusion 200 g/L, glucose 20.0 g/L, agar 15.0 g/L), and incubated at 28 °C for 2–3 d, until bacterial or fungal growth was started on the cut rhizome portions.

The obtained endophytes were inoculated in the corresponding liquid medium for 2–3 d to prepare fermentation broth, and after being centrifuged at 4000 r/min, the supernatant was taken, which was named cell-free supernatant (CFS). In this work, the antimicrobial capacity of the isolated endophytes was measured by Oxford cup method using *E. coli*, *S. aureus*, and *B. subtilis* (Yang et al., 2025). Among the isolated endophytes, the strain HJ9 with good antibacterial activity, was selected for subsequent experiments.

2.2. Preparation of CFS of the isolated strain HJ9 from P. cyrtonema Hua

The frozen strain HJ9 was thawed, and streaked it onto PDA plates to activate it. Afterwards, a single colony was selected, and inoculated in the basic PDB medium (potato infusion 200 g/L, glucose 20.0 g/L). After incubation at 160 r/min, 28 °C for 16 h, the seed culture was obtained, and then inoculated into the fermentation medium (potato infusion 200 g/L, glucose 30.0 g/L, yeast extract 7.5 g/L, KH_2PO_4 0.80 g/L) at an inoculum size of 2.0 %. After incubation at 160 r/min, 28 °C for 44 h, the fermentation broth was obtained. The fermentation broth was subsequently centrifuged at 4000 r/min for 10 min, and the supernatant was filtered through a 0.22 μm membrane to obtain CFS of strain HJ9.

2.3. Obtaining the degenerated strain of HJ9

A single colony of strain HJ9 was inoculated into PDB medium, and cultured at 28 °C, 160 r/min for 16 h. After that, the seed culture was obtained. The seed culture of HJ9 was then added to the new PDB medium with 2.0 % inoculum size as two generations of bacteria, and continued to be cultured for 2 d at 28 °C, 160 r/min. Repeat the above steps, a total of 54 generations of experiments were carried out. Antibacterial activity was assessed for each generation of the strains, and the decline in inhibitory activity was analyzed. Successive generations were cultured until the antibacterial activity of HJ9 against indicator bacteria, *E. coli* and *S. aureus*, was completely disappeared (Zhang et al., 2023b). The antibacterial activity was detected according to Oxford cup method. After 54 successive generations, completely degenerated strain dHJ9 was obtained, and preserved in glycerol tubes.

2.4. Morphological and molecular identification of the strains

The isolated bacterial strain HJ9 and the corresponding degeneration strain HJ9 were characterized by observing colony morphology. The strains were observed under an optical microscope after Gram staining (Coico, 2005).

For molecular analysis, the strains (HJ9 and dHJ9) were cultured in PDB medium for 24 h, and incubated at 28 °C, 160 r/min. The culture was then subjected to centrifugation at 4000 ×g for 10 min. The supernatant was discarded and the resulting cell pellet was then utilised for extracting genomic DNA, employing the Ezup column-based bacterial genomic DNA Extraction Kit (B518255), in accordance with the manufacturer's instructions. The strains were identified by the sequences of 16S ribosomal RNA (rRNA) genes. A sequence of approximately 1500 bp was successfully amplified from genomic DNA using primers 27 F and 1492 R, which were specifically designed for the

amplification of 16S ribosomal RNA genes. A 25 μL PCR reaction contained 1.0 μL (0.5–10.0 ng) of template DNA, 10 μM of each primer, 27 F (5'-AGAGTTTGATCMTGGCTCAG-3') and 1492 R (5'- GGTTACCTTGTTACGACTT −3'), dNTPs (each 10 mM), 10X PCR Buffer, 50 mM $MgSO_4$, and 5.0 U/μL Taq Plus DNA Polymerase. The cycle parameters were as follows: initial denaturation at 95 °C for 4 min; 30 cycles of denaturation for 30 sec at 94 °C, annealing for 30 sec at 57 °C, and extension for 90 sec at 72 °C; and a final overall extension for 10 min at 72 °C. The PCR product was then sent to Sangon Biotech (Shanghai, China) Co., Ltd. for sequencing. The sequences were subjected to a BLAST search against a database of homologous bacterial 16S ribosomal RNA sequences, as maintained by NCBI for analysis (Zhong et al., 2017).

2.5. Detection of pathogenicity of Fusarium sp. F2

The pathogenic fungus *Fusarium* sp. F2 used in this study was obtained from *P. cyrtonema* Hua tubers by our group, which was cultivated on PDA medium at 28 °C. Bacterial cake inoculation of isolated tubers method was used to determine the pathogenicity of *Fusarium* sp. F2 (Wang et al., 2025b). Healthy *P. cyrtonema* Hua tubers were selected, the surface of which was sterilized with 75 % ethanol. Afterwards, the tubers were carefully placed within a sterile box containing absorbent filter paper. After 7 d of incubation, the bacterial cake was taken, and inoculated to the wound. The inoculated sterile PDA fungus cake tubers were utilised as the control. All the samples were cultured at 25 °C for 6 d, and the incidence of the tubers was observed. The pathogenic bacteria were re-picked from randomly selected tubers, and the morphology was compared with that of the original inoculated strains. If it was the same as that of the original strains, it was indicated that the original strains were the pathogenic bacteria.

2.6. Comparison of the inhibitory activity of endogenous bacteria HJ9 and degenerate strain dHJ9 on Fusarium sp. F2

2.6.1. Dual culture assay

Using the dual culture assay, a mycelial plug (8 mm in diameter) of the pathogen was inoculated at the center of a PDA plate, while endophytes were point-inoculated at the edge of the same plate. Control plates were only inoculated with the pathogen. All plates were incubated at 28 °C for 5–7 d. Following the incubation period, the growth of the pathogen was documented in both the test and control groups. Based on these obtained results, the colony radius of the pathogen was measured in the test and control groups, and a comparison was made (Du et al., 2022).

2.6.2. Measurement of antifungal activity of endogenous bacteria HJ9 and degenerate strain dHJ9

Antifungal activity of CFS of HJ9 and dHJ9, was assessed using the poisoned food technique (He et al., 2014; Bedine et al., 2025). PDA plates were prepared containing CFS at concentrations of 0, 1.0 %, 5.0 %, 10 %, 15 %, 20 %, 25 %, 30 %, 35 %, 40 %, 45 %, 50 % (v/v). A mycelial plug with 8 mm in diameter, taken from a 7-day-old culture of *Fusarium* sp. F2, was placed at the center of each plate. Control plates containing PDA without CFS, were also inoculated. All plates were cultured at 28 °C for 7 d. The diameter of the colony was determined as the mean growth along two perpendicular lines. Antifungal activity was expressed as a percentage inhibition rate, which was calculated using the following formula:

$$\text{Inhibition rate (\%)} = ((R_c - R_p) / R_c) \times 100$$

Where R_c is the radial growth in the control, and R_p is the radial growth in the treated plates.

2.6.3. Measurement of spore germination rate

Sterile water was added into the activated *Fusarium* sp. F2 plates, and spores were then eluted off via agitation. The concentration of the spore suspension was subsequently diluted to achieve 1×10^7 CFU/mL. PDB medium containing varying contents of CFS (0, 12.5 %, 25 %, 50 % (v/v)) was prepared and mixed thoroughly with the pathogenic spore suspension at a 1:1 ratio. The cultures were then left to incubate at 28 °C for 7 h, with regular counts conducted every 1 h. After the completion of the incubation, the spores were eluted off and counted, and the spore germination rate was calculated by microscopic observation method (He et al., 2025; Zhang et al., 2023a).

Spore germination rate (C) was calculated using the following formula:

$$C(\%) = (C_1/C_2) \times 100$$

Where the total number of microscopically examined spores is C_2, and the number of germinated spores is C_1.

2.6.4. Determination of protein and nucleic acid leakage

The experiments were performed following the methods described by Jiao et al. (2020) and He et al. (2025) with slight modifications. 100 μL of *Fusarium* sp. F2 spore suspension (1×10^7 spores/mL) was transferred to conical flasks containing 100 mL PDB medium, and incubated at 160 r/min, 28 °C for 3 d. After the incubation, mycelia were collected via centrifugation at 4000 r/min for 10 min, after which they were thoroughly washed with sterile distilled water. The obtained fresh mycelium was re-suspended in CFS of endophytic bacteria at different concentrations adjusted into 0, 12.5 %, 25 %, 50 % (v/v). The suspension was incubated at 160 r/min, 28 °C, where 100 μL was collected every 12 h. The suspension was centrifuged at 4000 r/min for 10 min. The supernatant was obtained, and the absorbance values were conducted at 260 and 280 nm, respectively, with the employment of a UV spectrophotometer (Thermofisher, China).

2.6.5. Evaluation of plasma membrane integrity

100 μL of *Fusarium* sp. F2 spore suspension (10^7 spores/mL) was added into PDB medium containing 0, 12.5 %, 25 %, 50 % (v/v) concentrations of CFS of endophytic bacteria HJ9 and dHJ9. The mixture was cultured at 28 °C for 4 d. The mycelium was collected, washed with PBS, and stained using a propidium iodide staining kit (Sangon Biotech, Shanghai, China). The staining was conducted at ambient temperature in a dark environment for a duration of 30 min. The samples were observed under a fluorescence microscope (Sun et al., 2020).

2.6.6. Detection of membrane lipid peroxidation

Malondialdehyde (MDA) level was measured using thiobarbituric acid (TBA) method (Botsoglou et al., 1994; Ren et al., 2024). The treated mycelia, obtained according to the method **2.6.5**, were ground in a mortar under liquid nitrogen. 2.0 mL of 10 % trichloroacetic acid (TCA) was added to a small amount of quartz sand, which was then subjected to grinding until a homogenate was formed. Subsequently, an additional 8.0 mL of TCA was added for further grinding. The homogenate underwent centrifugation for 10 min, after which the resulting upper layer was collected as the sample extract. 2.0 mL of the supernatant was then mixed with 2.0 mL of a 0.60 % TBA solution. This mixture was reacted in a boiling water bath for 15 min, rapidly cooled, and centrifuged again. The supernatant was collected, and its absorbance (A) was determined at wavelengths of 532 nm, 600 nm, and 450 nm, respectively. MDA content was calculated using the formula (Wu et al., 2018; Ren et al., 2024):

$$\text{MDA (μmol/kg)} = 6.45 \times (OD_{532} - OD_{600}) - 0.56 \times OD_{450}$$

2.6.7. In vitro biofilm formation assay

The experimental procedures were performed following the methods described by Peng et al. (2024) and Sav et al. (2018) with slight modifications. Spore suspensions (1×10^5 spores/mL) were obtained by the method described in the Section 2.6.3. Aliquots of 100 μL of the spore suspension were added to wells of a 96-well microtiter plate. Concurrently, 100 μL of endophyte CFS at different concentrations (0, 1.5625 %, 3.125 %, 6.25 %, 12.5 %, 25 %, 50 % (v/v)) was added to each well. The plates were then incubated statically at 28 °C for 24 h.

After the 24 h incubation, the culture medium was carefully aspirated and discarded. Each well was treated with 200 μL of methanol for 15 min. The methanol was then discarded, and the plates were air-dried. Afterwards, 200 μL of 0.10 % (w/v) crystal violet solution was added into each well and fostered at room temperature for staining 10 min. The crystal violet solution was aspirated, and the biofilms were washed three times with sterile water, followed by air-drying. To solubilize the bound crystal violet, 200 μL of 33 % (v/v) glacial acetic acid was added into each well and allowed to stand for 15 min. The resultant solution was subsequently transferred to a new 96-well microtiter plate. Absorbance at 570 nm (OD_{570}) was measured using a microplate reader.

The percentage reduction in biofilm formation capacity was calculated using the following formula: Percentage reduction (%) = (1 - [OD_{570} of test group / OD_{570} of control group]) × 100

2.6.8. Inhibitory effects on mature biofilms

The spore suspension (1 × 10^5 spores/mL) was prepared following the method described in the Section **2.6.3.** 100 μL of the suspension was aliquoted into wells of a 96-well microtiter plate. Subsequently, 100 μL of PDB medium was added into each well. The plate was then incubated statically at 28 °C for 24 h to allow mature biofilm formation (Tang et al., 2024). After the incubation, the culture medium was aspirated, and the biofilms were gently washed with sterile water. Then, 200 μL different concentrations of CFS (0, 12.5 %, 25 %, 50 % (v/v)) was added into each well, followed by static incubation at 28 °C for 24 h. Effect of CFS concentrations on mature pathogenic biofilms was evaluated using the crystal violet staining assay. The methodology was conducted following the Section 2.6.7.

2.6.9. In vivo activity evaluation of endophyte CFS

P. cyrtonema Hua rhizomes were soaked in endophyte CFS at the concentration of 25 % (v/v), as well as in sterile water (control), for 15 min. The rhizomes were air-dried in a laminar flow hood. A purified pathogen culture (*Fusarium* sp. F2) was inoculated onto the wounds of the rhizomes. The inoculated rhizomes were placed in sterilized storage boxes, which were cultured at room temperature. Observations were investigated every 2 d to monitor tissue changes and disease progression during storage (Ezzat et al., 2021).

2.6.10. Pot experiment biocontrol experiment

To evaluate the efficacy of endophyte HJ9 and its degenerate strain dHJ9 in controlling *P. cyrtonema* Hua root rot, pot experiments were conducted according to previous reports by Sha et al. (2025) and Liu et al. (2022) with some modifications. Specifically, *P. cyrtonema* Hua seedlings were transplanted into the pots. After the seedlings were stabilized, they were then divided into two parts: one part was left to grow naturally without treatment as the untreated control group; the other part was subjected to overnight root-damage immersion treatment with *Fusarium* sp. F2 suspension (prepared following the method **2.6.4**).

After disease symptoms were developed on the treated *P. cyrtonema* Hua seedlings, they were divided into 4 groups for root irrigation, with 6 pots per group. Group A: treated with 50 mL sterile water (Control). Group B: treated with 50 mL CFS of strain dHJ9. Group C: treated with 50 mL bacterial suspension of strain HJ9 (1 ×10^8 CFU/mL). Group D: treated with 50 mL CFS of strain HJ9. After 14 d of treatment, the disease index and relative biocontrol efficacy of *P. cyrtonema* Hua seedlings were assessed. Disease severity was rated on a 0–4 scale (Feng et al., 2025): Grade 0: no visible symptoms. Grade 1: slight wilting of leaves. Grade 2: plant showing wilting symptoms. Grade 3: plant yellowing, stunted, and wilting. Grade 4: plant dead. The disease index and relative biocontrol efficacy were calculated as follows:

Disease index = 100 × ∑(number of diseased plants in each grade/total number of plants investigated with the highest disease index)

Relative biocontrol efficacy(%) = (disease index of the control−disease index of the antagonist)/disease index of the control × 100

2.6.11. Determination of IAA production

After culturing endophyte HJ9 and its degenerate strain dHJ9 in liquid medium to the logarithmic growth phase, OD_{600} of the suspension was measured. The suspension was centrifuged at 10,000 r/min for 10 min, and 100 μL of the supernatant was mixed with an equal volume of Salkowski colorimetric reagent. The mixture was kept in the dark for 30 min, after which OD_{530} was measured (Ribeiro and Cardoso, 2012; Zeng et al., 2025). IAA secretion amount = C_{sample} / OD_{600}; C_{sample} = (OD_{530} − 0.04470) / 0.005017, where IAA secretion amount: the amount of IAA secreted per unit volume of the suspension when the cell concentration corresponds to OD_{600} = 1.0 (μg/mL); C_{sample}: the concentration of IAA in the samples, obtained from the linear regression equation of the standard curve (μg/mL).

2.6.12. Gene expression for lipopeptide antibiotic compounds

PCR amplification was performed using the genomic DNA of the strain as the template. Primers were designed for the genes *ItuA* (Iturin A synthetase gene), *FenB* (Fengycin synthetase gene), *SrfAB* (Surfactin synthetase gene), *bmyA* (Bacillomycin D synthetase gene), and *bamD* (*bamD* gene within Bacillaene biosynthetic gene cluster) (Zhang et al., 2019; Yang et al., 2024). The primer sequences were listed in Table 1. PCR reaction was carried out in a 50 μL system under the following conditions: 94 °C for 5 min; 30 cycles of 94 °C for 30 s, 58 °C for 30 s, and 72 °C for 1 min; followed by a final extension at 72 °C for 10 min. The PCR products were analyzed by 1.2 % agarose gel electrophoresis to verify the amplification of the target fragments.

The expression levels of the genes *ItuA*, *bamD*, *SrfAB*, and *bmyA* were evaluated by quantitative Real-Time PCR (qRT-PCR). The primer sequences used were listed in Table 1. Total RNA was extracted from bacterial samples according to the manufacturer's instructions. qRT-PCR was performed using SYBR Green Realtime PCR Master Mix as per the manufacturer's protocol. The *rplA* gene was used as the internal reference (primer sequences showed in Table 2; Cheng et al., 2024). The qRT-PCR program was as follows: 95 °C for 2 min; 40 cycles of 95 °C for 5 s and 60 °C for 15 s, with fluorescence signal acquisition at 60 °C. Gene expression was quantified using the $2^{-}\Delta\Delta CT$ method, where ΔCT = CT (sample) – CT (control), and CT represents the threshold cycle.

2.7. Data statistics and analysis

Excel 2021 software was used to analyse the data, and calculated the mean value and standard deviation. The statistical analysis was conducted using SPSS 27.0 software, and $P < 0.05$ was considered as significant difference. Origin 2021 and GraphPad Prism 10.1.2 were used for plotting.

3. Results and discussion

3.1. Isolation of endophytes from P. cyrtonema Hua

In this study, 359 endophytic bacterial strains were isolated from

Table 1
Primer sequence of lipopeptide antibiotic synthase associated gene amplification.

Primer	Sequence: 5′ to 3′	Product size (bp)
*Itu*A	F: TGCCAGACAGTATGAGGCAG R: CATGCCGTATCCACTGTGAC	885
*bam*D	F: ATGAACAATCTTGCCTTTTTATTTCC R: TTTTAAAATCCGCAATTCTTCCC	1203
*Srf*AB	F: GTTCTCGCAGTCCAGCAGAAG R: GCCGAGCGTATCCGTACCGAG	308
*bmy*A	F: AAAGCGGCTCAAGAAGCGAAACCC R: CGATTCAGCTCATCGACCAGGTAGGC	1200
*Fen*B	F: TACCAATCGCAATGTCGTGT R: CTTCGATTTCTAACAGCCGC	767

Table 2
RT-PCR primer sequences.

Primer	Sequence: 5′ to 3′	Product size (bp)
rplA	F: CGTGTGCTTGGACCAAAAGG R: TCGCCGATTGCTTTTTCCAC	80
ItuA	F: CAACTTCTCCCCGTCTTCTGA R: AATGCGAGGCTGCAGAGAAT	140
bamD	F: GAAAAGGGTGCGGCATACAC R: TCGCTGATCGAATTTCCGCT	179
SrfAB	F: ACTATAAAGCCGGCAGCGAG R: TACCTGCACGAAATAGGCCG	98
bmyA	F: CCGAGACCGATCCGAAATCC R: GTGATCCGCAGTCTTGGTGA	171

P. cyrtonema Hua, among which 56 strains exhibited good antimicrobial activity against common pathogens (*E. coli*, *S. aureus*, *B. subtilis*). Among them, strain HJ9 emerged as the most potent antagonist, showing stable inhibitory activity, and was subsequently identified as *B. amyloliquefaciens* (Fig. 1a). At present, several endophytic *Bacillus* strains have been isolated and characterized from *P. cyrtonema* Hua. Chi et al. (2019) isolated *B. velezensis* from *P. cyrtonema* Hua, which exhibited notable antagonistic activity against *F. oxysporum*, a primary pathogen responsible for *Polygonatum* root rot. Lyu et al. (2022) further confirmed that endophytic *B. velezensis* strain HJ-3 from *P. cyrtonema* Hua inhibited *F. oxysporum* and *F. graminearum* by 73.87 % and 72.16 %, respectively, reinforcing the potential of *Bacillus* species in controlling *Fusarium* spp. The Gram-positive biocontrol bacterium *B. amyloliquefaciens*, has showed great potential for managing crop diseases, owing to its broad-spectrum antimicrobial activity, environmental adaptability, and multiple growth-promoting mechanisms (Luo et al., 2022; Sun et al., 2025). Many investigations have showed that *B. amyloliquefaciens* can directly inhibit various pathogenic fungi (*e.g.*, *Fusarium* spp.), bacteria and nematodes by secreting lipopeptides, volatile organic compounds, and iron carriers, while also indirectly enhancing host defense through induced systemic resistance niches competition (Chen et al., 2007; Jamali et al., 2018; Wu et al., 2019; Xu et al., 2023b). According to the antibacterial activity of *B. amyloliquefaciens* HJ9 in this study, the strain represented a promising biocontrol candidate for *Polygonatum*-related diseases.

3.2. Obtaining the degenerate strain *B. amyloliquefaciens* dHJ9

To investigate the functional decline often observed in *Bacillus* species during subculturing, *B. amyloliquefaciens* HJ9 was subjected to 54 consecutive subcultures in this study. The resulting degenerate strain *B. amyloliquefaciens* dHJ9, completely lost its ability to inhibit *E. coli* and *S. aureus* (Fig. 1b). The phenomenon of microbial degeneration has been observed. Zhu and Yang (2000) reported that degenerate strains of *B. subtilis* significantly diminished antagonistic activity against pathogens such as *Rhizoctonia* spp. and *Penicillium* spp. The authors further found that the degeneration rate was strongly influenced by both the medium's nutritional composition and the strain's inherent genetic traits. Tang et al. (1996) found that *Beauveria bassiana* exhibited high genetic instability, leading to strain degeneration. The degeneration resulted in reduced virulence against *Pine processionary caterpillar*, and seriously compromising its efficacy as a biocontrol agent.

Comparative molecular analysis of *B. amyloliquefaciens* HJ9 and its degenerated strain dHJ9 revealed a 98.3 % sequence similarity, confirming that species-level identity was remained despite the loss of antagonistic activity. Similarly, in the study of Zhang et al. (2023b), the authors investigated molecular mechanisms underlying degeneration in *Cordyceps militaris*, and found that although the degenerate strain exhibited no genomic mutations, significant alterations in its gene expression profile were observed (*e.g.*, a 39.6 % upregulation in

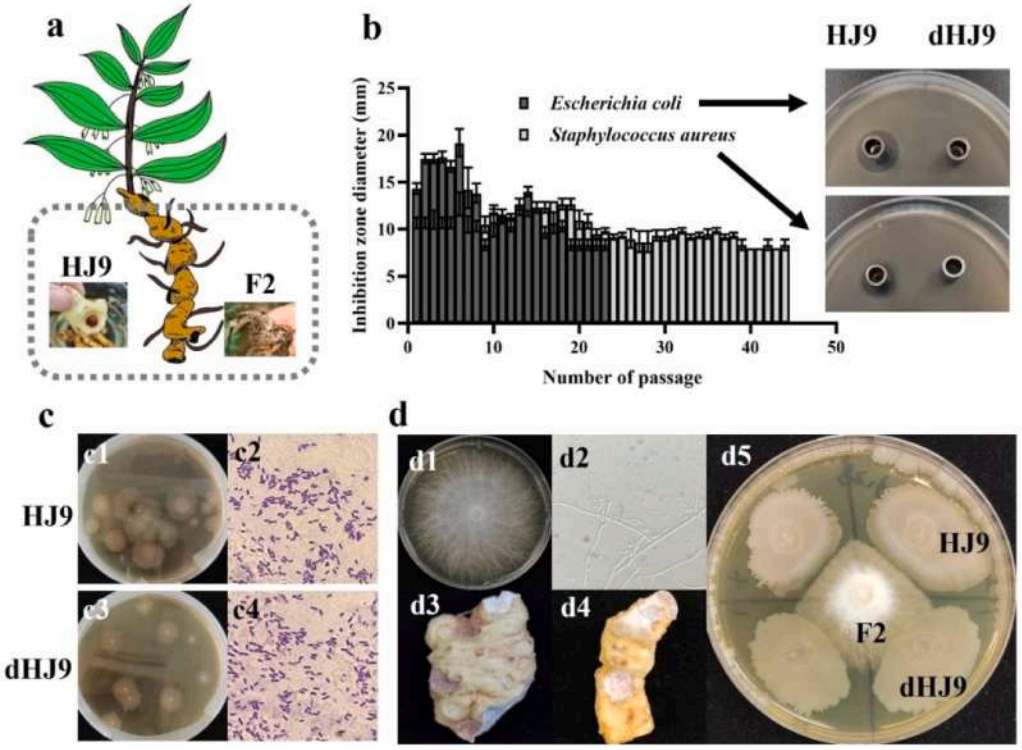

Fig. 1. The endophytic bacterium *B. amyloliquefaciens* HJ9 from *P. cyrtonema* Hua and its degenerate strain dHJ9. a. *P. cyrtonema* Hua sample; b. Changes in antibacterial activity of *B. amyloliquefaciens* strain HJ9 during subculture (*E. coli* and *S. aureus*); c. *B. amyloliquefaciens* HJ9 and degenerate strain *B. amyloliquefaciens* dHJ9: c1. Plate of *B. amyloliquefaciens* HJ9; c2. Gram staining of *B. amyloliquefaciens* HJ9; c3. Plate of degenerate strain dHJ9; c4. Gram staining of degenerate strain dHJ9; d. Pathogenic fungus *Fusarium* sp. F2: d1. plate of *Fusarium* sp. F2; d2. Mycelium and spores of F2 under optical microscope; d3. The control for pathogenicity test; d4. Pathogenicity test of *Fusarium* sp. F2; d5. Comparison of antagonistic effect of *B. amyloliquefaciens* HJ9 and degenerate strain dHJ9 against *Fusarium* sp. F2.

CCM_04090 gene expression), which ultimately led to reduced fruiting body formation and cordycepin production. This study revealed a significant difference in antibacterial activity between *B. amyloliquefaciens* dHJ9 and HJ9, supporting the viewpoint that strain degeneration could result in functional impairment. However, the underlying mechanisms responsible for this outcome remained unclear. To address this issue, our group has been employed PCR and qRT-PCR assays to monitor and compare the transcript levels of the key biosynthetic genes involved in antifungal compound (*e.g.*, lipopeptide synthetase genes) production between HJ9 and its degenerate counterpart, dHJ9.

As showed in Fig. 1c, clear morphological differences were evident between *B. amyloliquefaciens* HJ9 and its degenerate strain, dHJ9. Colonies of *B. amyloliquefaciens* dHJ9 exhibited a diminished central region and an expanded periphery containing substantial extracellular substances. This morphology might suggest impaired proliferative capacity, with the peripheral substances likely representing abnormal metabolites (*e.g.* exopolysaccharides, degradative enzymes), a phenomenon consistent with the abnormal residual nutrient consumption reported during *Cordyceps militaris* degeneration (Zhang et al., 2023b).

3.3. Detection of pathogenicity of Fusarium sp. F2

In our preliminary study, *Fusarium* sp. F2 was isolated from *P. cyrtonema* Hua affected by root rot. The morphological characteristics of *Fusarium* sp. F2 were showed in Figs. 1-d1, d2. The colony exhibited a fluffy texture, with dense and vigorous mycelium covering the surface. The mycelial mat was opaque and displayed a grayish-white coloration. The hyphae were slender, branched, grew robustly, presenting a cottony and appressed appearance. Conidiophores emerged from lateral branches, typically with 2–3 whorled branches, and were arranged singly, in pairs, or in clusters. The conidia were elliptical, formed at the hyphae tips, pale in color, featured smooth outer walls with fusiform ends. Microconidia were ovoid to reniform, aseptate, and had bluntly rounded apices.

After 6 d of inoculation with *Fusarium* sp. F2, the healthy rhizomes developed significantly more extensive lesions than those in the control group (Figs. 1-d3, d4). Therefore, our results confirmed the strong pathogenicity of *Fusarium* sp. F2. Various pathogens have been reported to cause root rot in *P. cyrtonema* Hua. Liang and Li (2021) isolated and identified pathogens from *P. cyrtonema* Hua in Hunan Province, China, who determined that *F. foetens* and *F. hostae* were primarily causes for root rot in this region. In the work of Han et al. (2020), the authors indicated that *F. oxysporum* and *F. solani* were responsible for root rot in *P. cyrtonema* Hua in Chongqing, China. Recently, Wang et al. (2023a) isolated 28 fungal strains from infected *P. cyrtonema* Hua samples, 12 of which induced significant root rot symptoms. Subsequent analysis based on morphological characteristics and phylogenetic tree construction identified these 12 pathogenic strains as *F. oxysporum*. Our findings were consistent with previous studies in establishing *Fusarium* spp. as a key pathogen in *P. cyrtonema* Hua root rot. However, the specific species identity of the highly pathogenic *Fusarium* sp. F2 strain used in this study requires further investigation.

3.4. Antifungal activity of B. amyloliquefaciens HJ9 and its degenerate strain B. amyloliquefaciens dHJ9 against Fusarium sp. F2

3.4.1. Dual culture assay

In dual-culture assays, the average growth inhibition rate of *B. amyloliquefaciens* HJ9 against *Fusarium* sp. F2 was 63.39 %. In comparison, the degenerate strain dHJ9 showed a reduced efficacy, with an average inhibition rate of 53.74 %. As illustrated in **Fig. 1d5**, a distinct inhibition zone was evident at the interface between *B. amyloliquefaciens* HJ9 and *Fusarium* sp. F2, whereas no such zone was observed with the degenerate strain dHJ9. The limited growth restriction of the pathogen that did occur was likely attributed to the rapid colonization by the degenerate strain of *B. amyloliquefaciens* dHJ9, which competed with *Fusarium* sp. F2 for spatial and nutritional resources. In the work of Palmieri et al. (2020), the authors demonstrated that *Rahnella aquatilis* suppressed *Fusarium* growth via environmental acidification mediated by gluconic acid secretion, and that the loss of this ability in *gcd* mutants largely abolished the antagonism. Here, the potent inhibition and distinct zone induced by *B. amyloliquefaciens* HJ9 suggested a similar mechanism potentially involving acidification or the secretion of antimicrobial metabolites that altered the microenvironment. Conversely, the absence of an inhibition zone by strain dHJ9 indicated a reduce in the antimicrobial activity, a phenotype consistent with the deficiency observed in *gcd* mutants of *Rahnella aquatilis* (Palmieri et al., 2020). Despite its reduced antifungal activity, *B. amyloliquefaciens* dHJ9 might have still limited pathogen proliferation by competing for nutrients, which aligned with the observations reported by Wu et al. (2025). Furthermore, Franco et al. (2025) observed that antagonistic interactions in fungal co-cultures (e.g., *Trichoderma* spp.) frequently activated defense-related metabolite production, leading to growth arrest zones. Therefore, the differential antagonism between *B. amyloliquefaciens* HJ9 and the degenerate strain dHJ9 was driven primarily by antibiosis through the production of bioactive metabolites.

3.4.2. Determination of the inhibitory rate of Fusarium sp. F2 mycelial growth

The antifungal activity of CFS of *B. amyloliquefaciens* HJ9 or its degenerate strain dHJ9 was evaluated by incorporating CFS into PDA solid medium and culturing *Fusarium* sp. F2 on it. As showed in Fig. 2a, the average colony diameter of *Fusarium* sp. F2 in the control group reached 78.8 mm after 7 d of incubation. In contrast, the addition of CFS from *B. amyloliquefaciens* HJ9 at concentrations of 0–50 %(v/v) resulted in a dose-dependent inhibition of mycelial growth, with significant reductions ranging from 20 % to 76 %, respectively ($P < 0.05$) (Fig. 2b). These results indicated that CFS from *B. amyloliquefaciens* HJ9 significantly inhibited the growth of *Fusarium* sp. F2 in a concentration-dependent manner. In contrast, CFS from the degenerate strain dHJ9 exhibited minimal inhibitory activity, with inhibition rates remaining near 0 % ($P = 0.1975$) even at at the highest concentration of 50 % (v/v). The poor antifungal activity of CFS of *B. amyloliquefaciens* dHJ9 demonstrated that this degenerate strain lost the capacity to secrete antifungal components. Such components, likely acted by destroying fungal cell structures. Yi et al. (2024) confirmed that lipopeptides could induce hyphal swelling and deformation. In the work of He et al. (2025), the authors observed that treatment with oleuropein and matrine caused morphological damage, such as shrinkage and breakage in *Fusarium* sp. hyphae, which was accompanied by the leakage of intracellular nucleic acids and proteins. In our present study, CFS of *B. amyloliquefaciens* HJ9 strongly inhibited the growth of *Fusarium* sp. F2, reducing colony diameter by up to 76 %. This suggested that its active components might suppress hyphal extension, potentially via the disruption of the cell membrane structure. In the work of Saikia et al. (2025), the authors demonstrated that the antifungal properties of microorganisms were closely linked to the integrity of their secondary metabolic gene clusters. The loss or inactivation of these clusters could lead to a decrease of antifungal capability (*e.g.*, interruption of secondary metabolite synthesis). In this study, the degenerate strain *B. amyloliquefaciens* dHJ9 showed no inhibitory activity even at high CFS concentrations, suggesting that it might have lost the ability to synthesize lipopeptides or key extracellular enzymes as a result of genetic degeneration. This findings were also consistent with the report by Yi et al. (2024), which emphasized the necessity of functional biosynthetic pathways for the antifungal action of *B. amyloliquefaciens* strain ZK-9.

3.4.3. Determination of inhibition rate for Fusarium sp. F2 spore germination

As showed in Fig. 2c, the inhibition rate of CFS of *B. amyloliquefaciens* HJ9 on *Fusarium* sp. F2 spore germination was concentration-dependent, with higher CFS concentrations leading to greater

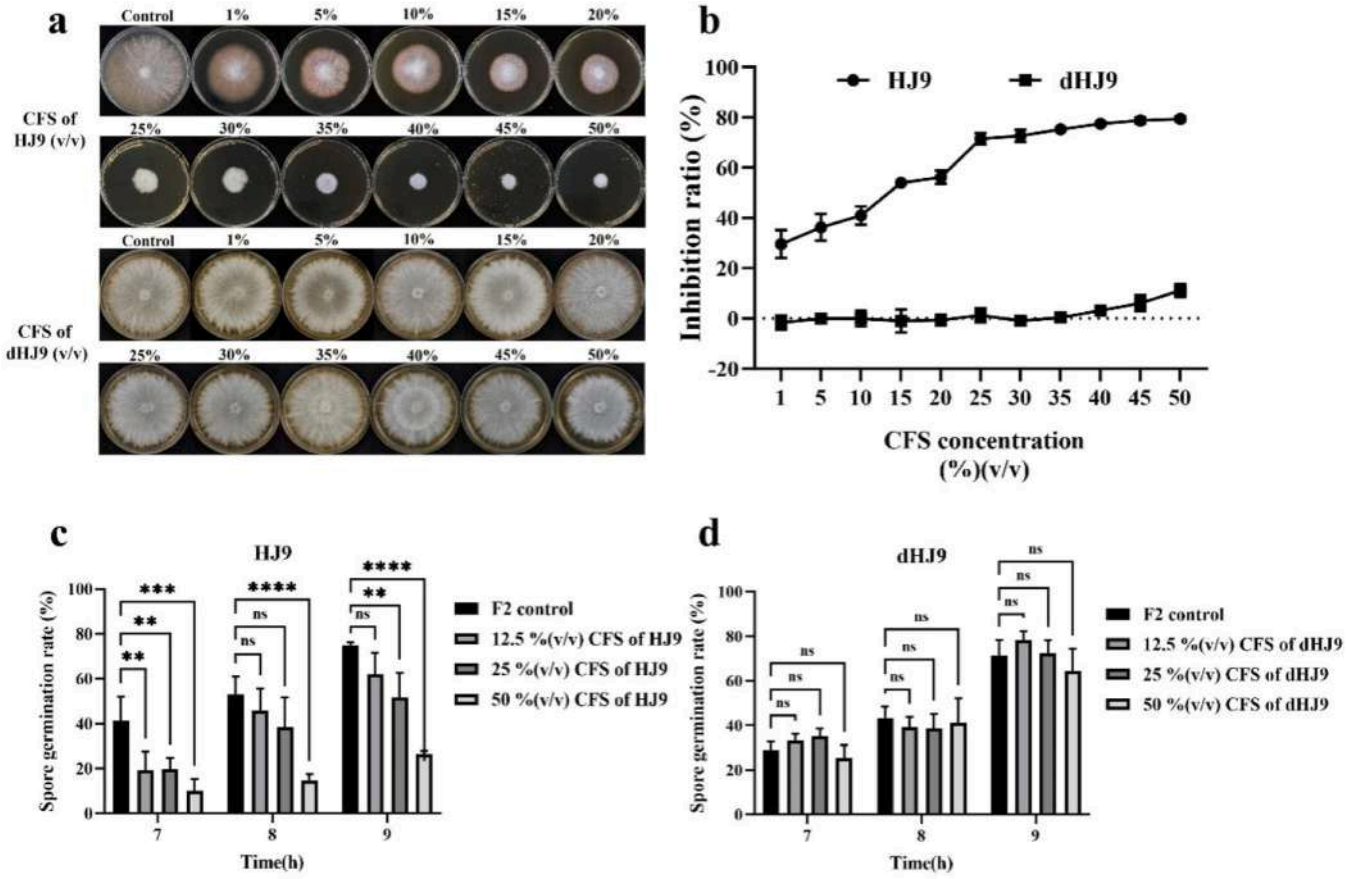

Fig. 2. The inhibitory effects of *B. amyloliquefaciens* HJ9 and the degenerate strain dHJ9 on the growth of *Fusarium* sp. F2. a. Mycelial growth patterns after 7 days of incubation at 28 °C. b. Effect of different concentrations of CFS of *B. amyloliquefaciens* HJ9 and the degenerate strain dHJ9 on the inhibition rate of mycelial growth of the pathogen. c. Effect of different concentrations of CFS of *B. amyloliquefaciens* HJ9 on the germination rate of *Fusarium* sp. F2 spores. d. Effect of different concentrations of CFS from the degenerate strain *B. amyloliquefaciens* dHJ9 on the germination rate of *Fusarium* sp. F2 spores. Data are the mean ± standard error (n = 3). Asterisks indicated significant differences between the control and experimental groups as determined by the spore germination rate test (**p < 0.01, *p < 0.001, ****p < 0.0001), and ns indicated no significant difference.

inhibition. At 50 % (v/v)CFS, a strong inhibitory activity was observed, reaching 74 % inhibition rate after 7 h and remaining a substantial level of 64 % by 9 h. These results indicated that CFS exhibited both rapid and sustained antifungal efficacy. In contrast, at a low concentration (12.5 %, v/v), CFS showed a comparatively weaker inhibition rate (49 % at 7 h), which decreased markedly to 19 % by 8 h, indicating that the inhibitory effect was only transient under low-concentration conditions. In short, during the investigated time, the inhibition rate declined across all concentration groups, through this decrease was notably more persistent in the high-concentration group. In contrast, CFS of the degenerate strain *B. amyloliquefaciens* dHJ9 exhibited no significant difference in spore germination inhibition between high and low concentrations (Fig. 2d), indicating a lack of concentration-dependent effect. These results demonstrated that the bioactive compounds secreted by the degenerate strain *B. amyloliquefaciens* dHJ9 were ineffective in suppressing *Fusarium* sp. F2 spore germination. The reason might that the loss or inactivation of the active compounds was due to the degeneration.

Hari et al. (2024) found that *Origanum elongatum* extract at a high concentration (20 mg/mL) inhibited *F. oxysporum* spore germination by 73.58 %. In our present study, CFS of *B. amyloliquefaciens* HJ9 at high concentration also exhibited potent and sustained inhibition of *Fusarium* sp. F2 spore germination, a pattern consistent with the prolonged antifungal effect reported by Hari et al. (2024) for high-concentration oregano extract against *F. oxysporum* spores. The dose-dependent inhibition of tomato *Fusarium* wilt by crude protein of *B. siamensis* QN$_2$MO-1 was reported by Zhang et al. (2024b). The findings in this work also indicated that the antifungal active compounds produced by *B. amyloliquefaciens* HJ9 required reaching a threshold concentration to exert stable effect. In the study of Wang et al. (2025a), the authors observed that saponins strongly inhibited *Fusarium* fungi mycelial growth at high concentrations, but had poor efficacy or even stimulated spore germination at low concentrations. The transient inhibitory effect of CFS of *B. amyloliquefaciens* HJ9 at low doses was also observed in this work.

3.4.4. Determination of protein nucleic acid leakage

As showed in Fig. 3a, under high concentrations (50 % (v/v)) of *B. amyloliquefaciens* HJ9 CFS, there was a significant increase in the leakage of nucleic acids and proteins from *Fusarium* sp. F2. In contrast, under lower concentrations (12.5 % (v/v) and 25 % (v/v)) of *B. amyloliquefaciens* HJ9 CFS, no significant differences in cellular leakage were observed in *Fusarium* sp. F2. Additionally, at all concentrations tested, CFS of the degenerate strain *B. amyloliquefaciens* dHJ9 induced negligible changes in nucleic acid and protein leakage from *Fusarium* sp. F2 (Fig. 3b).

Treatment with a high concentration (50 % (v/v)) of *B. amyloliquefaciens* HJ9 CFS caused a sustained increase in the leakage of nucleic acid and protein from *Fusarium* sp. F2 over the period of 12 h to 96 h (Fig. 3a). This results suggested that the antimicrobial substances from *B. amyloliquefaciens* HJ9 destroyed the integrity of the indicator strain cell membrane. In the study of Yan et al. (2023), the authors demonstrated that 100 μg/mL ferulic acid significantly damaged the cell membrane of *F. graminearum*, leading to elevated electrical conductivity,

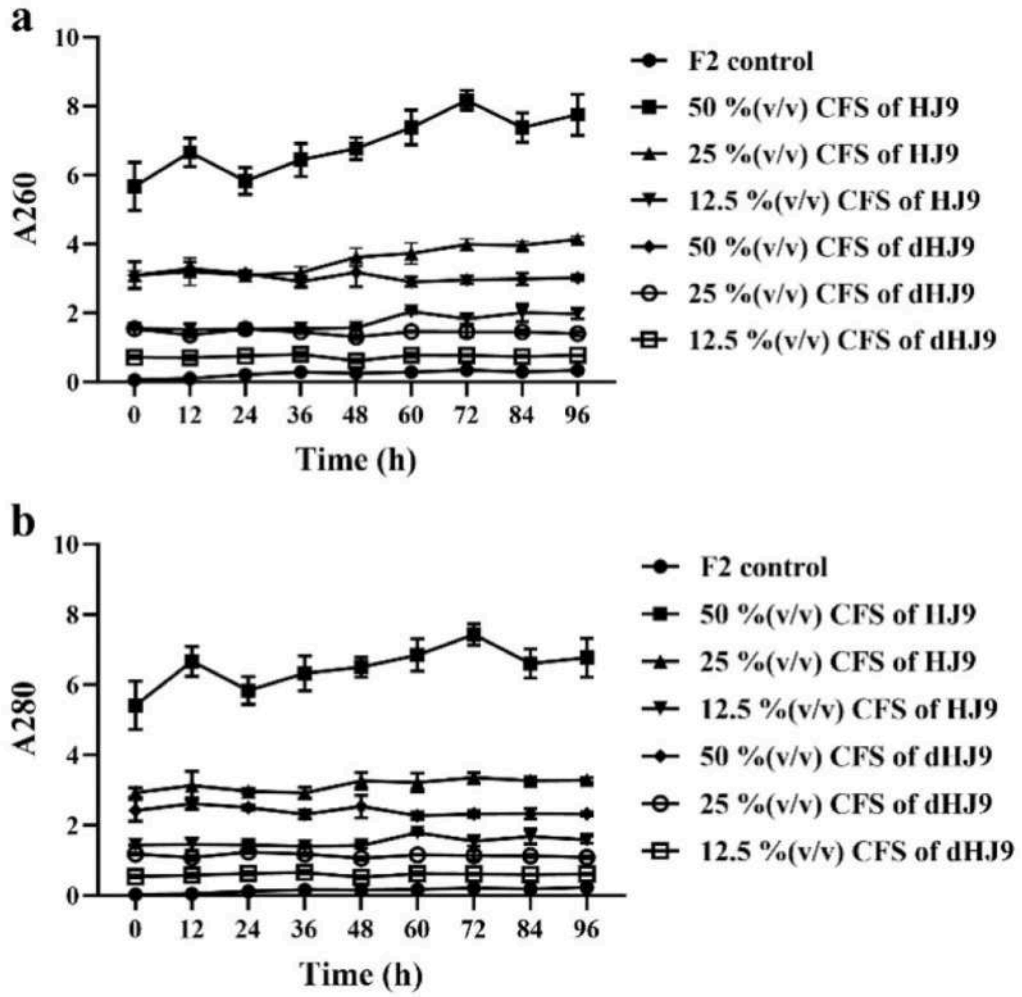

Fig. 3. Determination of protein and nucleic acid leakage in *Fusarium* sp. F2. a. Effect of CFS of *B. amyloliquefaciens* HJ9 and its degenerate strain dHJ9 on nucleic acid leakage of *Fusarium* sp. F2; b. Effect of CFS of *B. amyloliquefaciens* HJ9 and its degenerate strain dHJ9 on protein leakage of *Fusarium* sp. F2.

a 4-fold increase in nucleic acid leakage, and nearly a 2-fold higher in protein leakage. Similarly, Jiao et al. (2020) reported that ε-poly--L-lysine (200–400 mg/L) induced a sharp 3.6–4.7-fold surge in protein leakage in *Botrytis cinerea* within 2 h. Recently, Meng et al. (2024) confirmed that perillaldehyde could enhance cell membrane permeability of *F. graminearum*, causing increased electrical conductivity and the leakage of soluble sugars, nucleic acids, and proteins. In this study, the findings demonstrated that the antifungal activity of *B. amyloliquefaciens* HJ9 primarily operated through targeted disruption of the cell membrane, as evidenced by the sustained leakage of nucleic acids and proteins under high-concentration CFS treatment. In contrast, neither low concentrations (12.5 %, 25 %) of *B. amyloliquefaciens* HJ9 CFS nor the degenerate strain dHJ9 induced significant membrane damage, likely due to insufficient production of active antifungal components.

3.4.5. Evaluation of plasma membrane integrity

Propidium iodide is a fluorescent DNA-binding dye that enters cells with compromised plasma membrane integrity, producing red fluorescence upon binding to nuclear DNA (Sun et al., 2020). As showed in Fig. 4, *Fusarium* sp. F2 hyphae treated with CFS from the degenerate strain *B. amyloliquefaciens* dHJ9 exhibited only minimal PI staining, indicating largely intact cell membranes, and low levels of cell death or damage. However, treatment with *B. amyloliquefaciens* HJ9 CFS resulted in substantial PI staining, the intensity of which increased in a concentration-dependent manner. This demonstrated severe membrane damage and elevated cell mortality in *Fusarium* sp. F2, further confirming the consistency between the PI staining results and the previously observed leakage of protein and nucleic acid (Fig. 3). Both ferulic acid and perillaldehyde inhibited pathogenic fungi by disrupting membrane integrity, increasing permeability, and elevating PI fluorescence intensity (Yan et al., 2023; Meng et al., 2024). These results were consistent with the concentration-dependent increase in red fluorescence observed in PI-stained *Fusarium* sp. F2 hyphae treated with *B. amyloliquefaciens* HJ9 CFS. Collectively, the results confirmed the detrimental impact of *B. amyloliquefaciens* HJ9 CFS on both cellular function and membrane integrity in *Fusarium* sp. F2.

3.4.6. Determination of MDA content

The integrity, fluidity, and selective permeability of cell membrane are vital for microbial growth and pathogenicity. The accumulation of MDA, a byproduct of lipid peroxidation, serves as an indicator of cell membrane damage (Zhang et al., 2024a). Under treatment with CFS of *B. amyloliquefaciens* HJ9 and its degenerate strain dHJ9, MDA content in *Fusarium* sp. F2 exhibited distinct variations compared to the control (Fig. 5). *B. amyloliquefaciens* HJ9 CFS treatment resulted in a significant, concentration-dependent increase in MDA levels at all tested concentrations, whereas the degenerate strain dHJ9 caused no notable change. This suggested that *B. amyloliquefaciens* HJ9 enhanced its inhibition against *Fusarium* sp. F2 by promoting lipid peroxidation of the cell membrane. These findings were in accordance with the results of Meng et al. (2024) and Pan et al. (2025). In contrast, treatment with

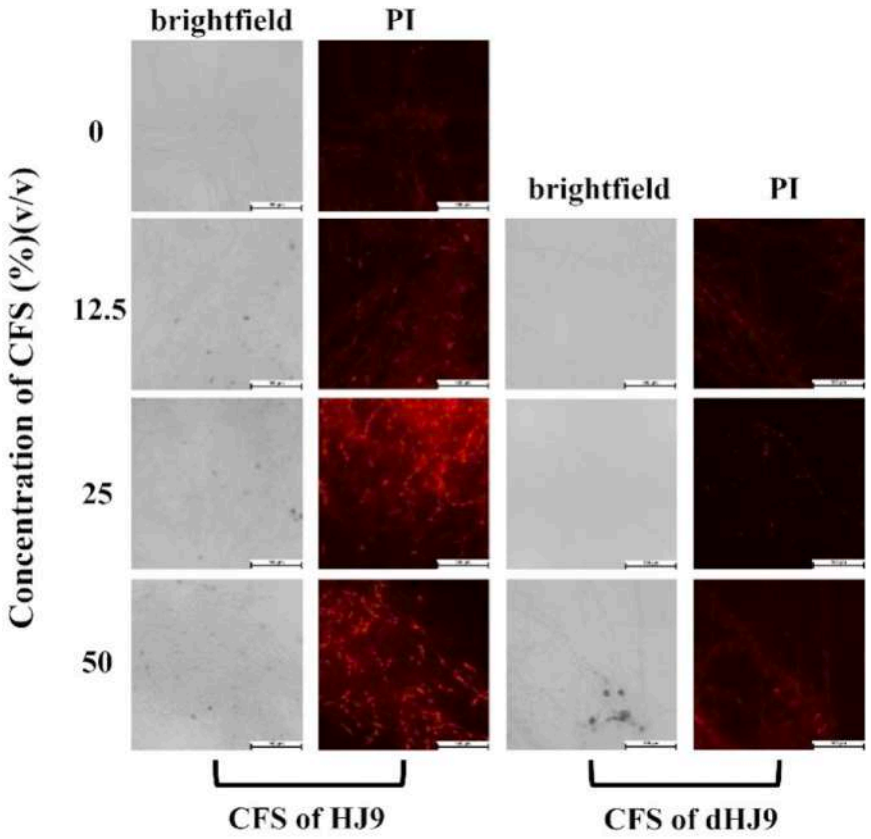

Fig. 4. PI staining observation of mycelia. At 28 ± 1 °C, *Fusarium* sp. F2 was exposed to different concentrations of *B. amyloliquefaciens* HJ9 and its degenerate strain dHJ9 CFS for 4 d, and cell membrane integrity was detected.

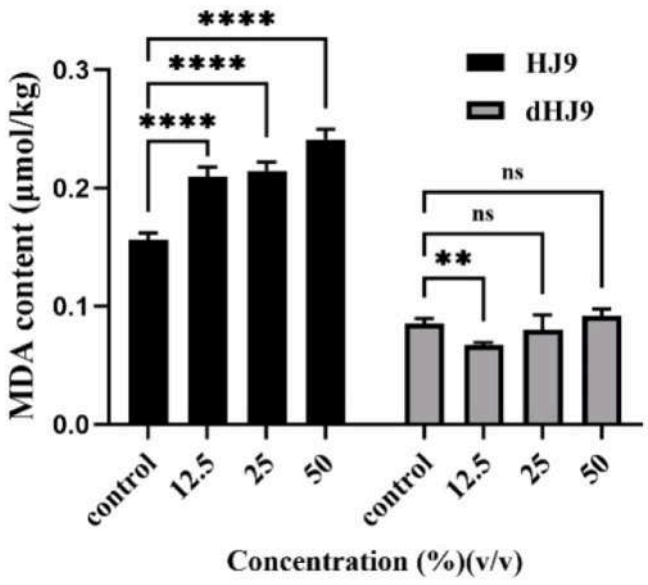

Fig. 5. Effects of CFS concentrations from *B. amyloliquefaciens* HJ9 and its degenerate strain dHJ9 on MDA content of *Fusarium* sp. F2. Expose *Fusarium* F2 mycelium to different concentrations of *B. amyloliquefaciens* HJ9 and its degenerate strain dHJ9 CFS at 28 ± 1 °C for 4 d, and measure MDA levels. Data are the mean ± standard error (n = 5). Asterisks indicated significant differences between the control and experimental groups as determined by the determination of MDA content (**p < 0.01, *p < 0.001, ****p < 0.0001), and "ns" indicated no significant difference.

B. amyloliquefaciens dHJ9 CFS resulted in only marginal increases in MDA content at lower concentrations (12.5 % (v/v) and 25 % (v/v)), with no significant difference observed at 50 %(v/v) compared to the control. This indicated a minimal impact of *B. amyloliquefaciens* dHJ9 CFS on the cell membrane. *B. amyloliquefaciens* HJ9 could efficiently inhibit *Fusarium* sp. F2 through a concentration-dependent pathway involving the induction of membrane lipid peroxidation. The degenerate strain *B. amyloliquefaciens* dHJ9, however, likely suffered from reduced production of antimicrobial substances (*e.g.*, lipopeptides) capable of causing membrane damage, and consequently lost its antifungal activity, potentially due to the downregulation of secondary metabolite synthesis genes (Pan et al., 2025).

3.4.7. Biofilm inhibition and eradication assays

As showed in Fig. 6a, the inhibitory effect of *B. amyloliquefaciens* HJ9 CFS on *Fusarium* sp. F2 biofilm formation increased in a concentration-dependent manner. At the highest concentration (50 % v/v) of CFS, the inhibition rate reached approximately 63 %. The inhibitory effect was reduced with the decrease of the concentrations, dropping to ~7 % at 6.25 % (v/v), with no significant inhibition observed at lower concentrations. In contrast, CFS of the degenerate strain *B. amyloliquefaciens* dHJ9 exhibited weaker inhibition rate of *Fusarium* sp. F2 biofilm formation, showing only ~40 % inhibition at 50 % (v/v) and declining rapidly to negligible levels at lower concentrations. Fig. 6**b** showed that neither *B. amyloliquefaciens* HJ9 nor the degenerate strain *B. amyloliquefaciens* dHJ9 CFS significantly eradicated mature *Fusarium* sp. F2 biofilms at any tested concentrations, indicating limited efficacy against established biofilms.

Biofilm formation proceeds through four key stages: adhesion, hyphal development, maturation, and dispersal (Pereira et al., 2021). Among these, the initial adhesion of planktonic cells to surfaces and subsequent hyphal differentiation from spores are particularly critical for biofilm establishment and pathogenesis (Huang et al., 2020; Zhang

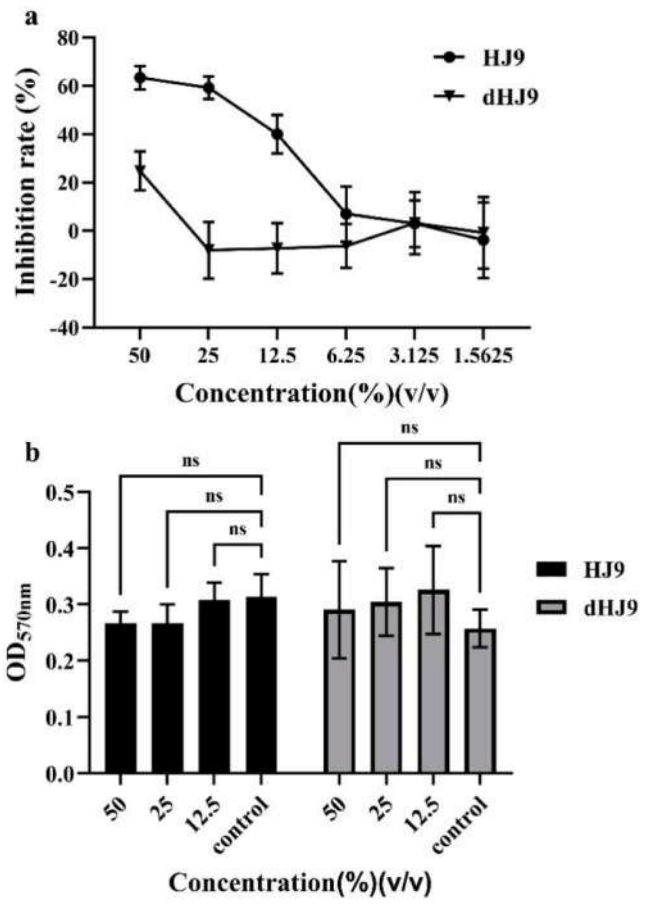

Fig. 6. Effects of CFS concentrations of *B. amyloliquefaciens* HJ9 and its degenerate strain dHJ9 on biofilm formation (a) and eradication of mature biofilms (b) in *Fusarium* sp. F2. The line graph showed the reduction rate of biofilm-forming ability in *Fusarium* sp. F2 after treatment with CFS of *B. amyloliquefaciens* HJ9 or its degenerated strain dHJ9 at different concentrations. The bar graph showed the absorbance (OD_{570}) of crystal violet-stained biofilms in *Fusarium* sp. F2 after 24 h of treatment with CFS of *B. amyloliquefaciens* HJ9 or its degenerate strain dHJ9 at different concentrations on pre-formed mature biofilms. Data represented the mean ± standard error (n = 5). "ns" indicated no significant difference.

et al., 2022). The adhesion stage initiates surface colonization, while hyphal development facilitates structural consolidation and invasion, thereby playing a decisive role in the infection process. In this study, *B. amyloliquefaciens* HJ9 CFS (12.5–50 % v/v) significantly inhibited *Fusarium* sp. F2 biofilm formation, reducing biomass by up to 63 % at 50 % (v/v). This suggested that *B. amyloliquefaciens* HJ9 metabolites primarily interfered with early-stage processes (adhesion or hyphal morphogenesis) during biofilm formation. This was consistent with its previously observed capacity of *B. amyloliquefaciens* HJ9 CFS to inhibit *Fusarium* sp. F2 spores germination (Fig. 2c). In contrast, the limited eradication of mature biofilms likely reflected structural resilience provided by the extracellular polymeric substance (EPS), which impeded antimicrobial penetration, in addition to the inherent complexity and tolerance of fungal biofilm (Aflakian and Hashemitabar, 2025). The eradication of mature biofilms poses a major challenge in antifungal biocontrol, as their dense EPS matrix forms a significant physical and chemical barrier (Lin et al., 2025). In our group, we have been developing a multi-mechanistic, synergistic strategy that combined *B. amyloliquefaciens* HJ9 CFS with other natural compounds possessing biofilm-disrupting activity, which might be key to overcoming biofilm-mediated tolerance.

Shay et al. (2022) demonstrated that early biofilm development in *F. graminearum* depended on EPS and nucleic acid deposition, with oxidative stress triggering adaptive hyphal responses. The potent inhibition by *B. amyloliquefaciens* HJ9 CFS might due to interference with EPS/nucleic acid synthesis, or disruption of cellular adhesion. Conversely, the reduced efficacy of the degenerate strain *B. amyloliquefaciens* dHJ9 indicated loss of key antimicrobial agents (*e.g.*, cell wall–disrupting lipopeptides or hydrolases) or a diminished capacity to mitigate biofilm-inducing reactive oxygen species.

3.4.8. *In vivo activity evaluation of endophyte CFS*

Tissue analysis revealed that lesions on *P. cyrtonema* Hua rhizomes in the sterile water (control) group progressively worsened within the first 6 days (Fig. 7). In contrast, the rhizomes treated with *B. amyloliquefaciens* HJ9 CFS showed significantly milder symptom; *Fusarium* sp. F2 inoculum disc exhibited minimal growth beyond the wound site, indicating effective inhibition by *B. amyloliquefaciens* HJ9 CFS during the initial stage. After the treated time at 8 d, control rhizomes were extensively colonized by *Fusarium* sp. F2 mycelium, with approximately two-thirds showing visible decay. Conversely, in rhizomes treated with *B. amyloliquefaciens* HJ9 CFS, the growth of *Fusarium* sp. F2 mycelium was confined to within 5 mm of the inoculation point, further confirming the strong antifungal efficacy of CFS treatment. Tiwari et al. (2020) demonstrated that non-pathogenic endophytes from potato phyllosphere and rhizosphere effectively suppressed dry rot pathogens, including *F. sambucinum* and *F. solani*. Furthermore, Zhang et al. (2024b) reported that the metabolites from *Bacillus siamensis* QN_2MO-1 interacted with tomato plants, potentially influencing phytohormone production levels. These hormones, such as auxins, gibberellins, and cytokinins, affected fruit development and ripening processes, and could induce plant immunity. The effective inhibition of *Fusarium* sp. F2 spread within the first 6 days by *B. amyloliquefaciens* HJ9 CFS treatment in this study suggested that *B. amyloliquefaciens* HJ9 CFS contained potent antifungal compounds, and might also produce bioactive substances that interacted with *P. cyrtonema* Hua rhizomes, significantly enhancing plant growth and inducing disease resistance.

Compared to the control, rhizomes treated with the degenerate strain *B. amyloliquefaciens* dHJ9 CFS exhibited a discernible but considerably weaker inhibitory effect against *Fusarium* sp. F2 than those treated with *B. amyloliquefaciens* HJ9 CFS. However, secondary infections caused by other pathogens were observed around the inoculation sites on rhizomes treated with the degenerate strain, indicating its compromised biocontrol capacity. Xue et al. (2019) demonstrated that T-2 toxin produced by biocontrol agents, could activate the phenylpropanoid metabolic pathway in plants, thereby enhancing tuber disease resistance. The increased susceptibility of *B. amyloliquefaciens* dHJ9 CFS-treated rhizomes to secondary infection was likely attributable to reduced secretion of signaling molecules (*e.g.*, lipopeptides, polyketides) by the degenerate strain that were crucial for inducing systemic resistance in *P. cyrtonema* Hua. This observation was consistent with the mechanism indicated by Wang et al. (2025a), where microbial interaction imbalances could trigger secondary diseases.

3.4.9. *Pot experiments for biological control*

As showed in Fig. 8 and Table 3, both *B. amyloliquefaciens* HJ9 and its CFS demonstrated a significant protective effect against *Fusarium*-induced root rot in *P. cyrtonema* Hua. CFS of *B. amyloliquefaciens* HJ9 exhibited particularly optimal efficiency, achieving a control efficiency of 67.86 % and reducing the disease index to a level comparable to the control group. While the bacterial suspension of *B. amyloliquefaciens* HJ9 also reduced root rot severity compared to the positive control (infected untreated), its efficacy was weaker than that of CFS, achieving a control efficiency of 28.57 %. Conversely, CFS of the degenerate strain *B. amyloliquefaciens* dHJ9 might exacerbate root rot, as reflected by a higher disease index than the positive control.

The superior disease control efficacy of *B. amyloliquefaciens* HJ9 CFS compared to the bacterial suspension group, might be attributed to

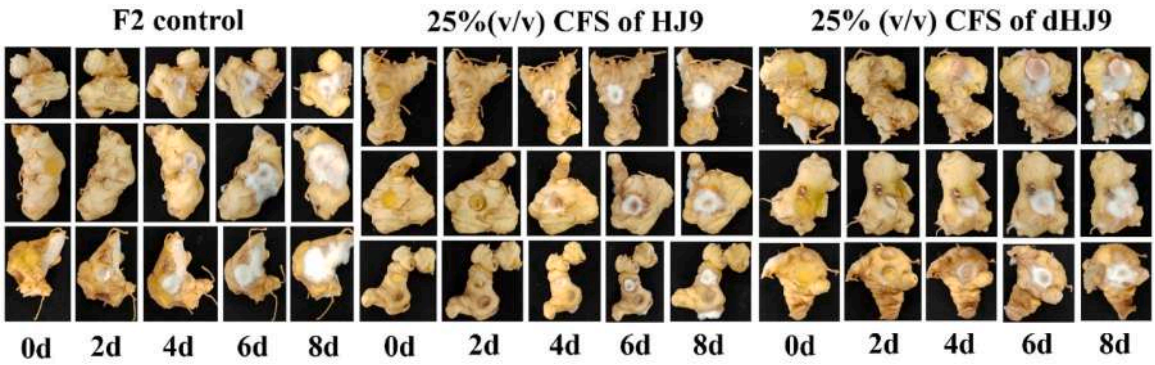

Fig. 7. *In vivo* antifungal activity assay of *B. amyloliquefaciens* HJ9 and its degenerate strain dHJ9 CFS against *Fusarium* sp. F2 on *P. cyrtonema* Hua rhizomes. Rhizomes were treated by immersion for 15 min in either: (1) sterile water (control), (2) 25 % (v/v) CFS of *B. amyloliquefaciens* HJ9, or (3) 25 % (v/v) CFS of the degenerate strain dHJ9. Following treatment, the rhizomes were inoculated with *Fusarium* sp. F2 mycelial plugs. The appearance of the rhizomes was visually assessed every 2 days.

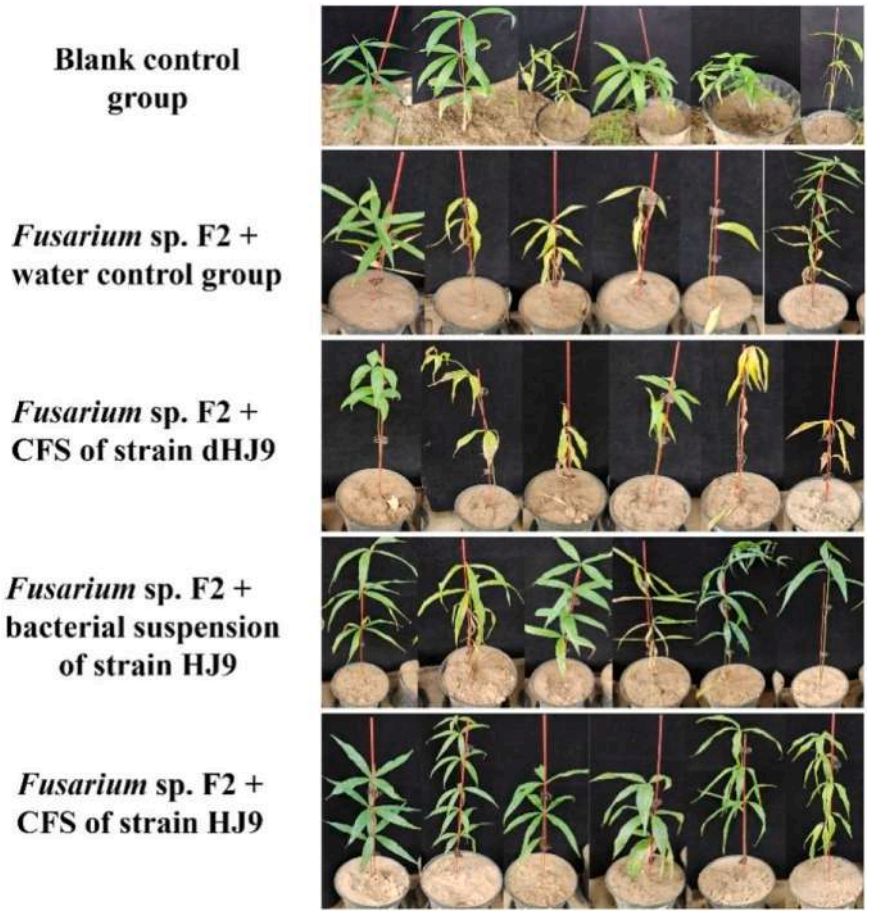

Fig. 8. Results of the pot experiments. The blank control group was allowed to grow naturally without treatment; the other groups were treated by soaking the roots in a suspension of *Fusarium* sp. F2 overnight. After 7 d of *Fusarium* sp. F2 colonization, each group's samples (Water control; 50 mL of CFS from strain *B. amyloliquefaciens* dHJ9; 50 mL of bacterial suspension from strain *B. amyloliquefaciens* HJ9 (1×10^8 CFU/mL); 50 mL of CFS from strain *B. amyloliquefaciens* HJ9) were applied to the soil, and the results were observed 15 days after planting.

higher concentrations of active metabolites, enabling rapid inhibition of *Fusarium* sp. F2 growth. In contrast, the bacterial suspension depended on successful colonization and *in situ* metabolite production, whose efficiency was influenced by environmental factors (*e.g.* soil pH and nutritional competition) and the strain's colonization capability (Sun et al., 2025).

In the work by Sun et al. (2025), CFS of *B. velezensis* GX1 was rich in antimicrobial metabolites, such as lipopeptides, and could act directly suppressed pathogens. Compared to *B. velezensis* GX1, the strain *B. velezensis* GX8 showed the lower antibacterial activity due to lower lipopeptide production. It was similar to the degenerate strain *B. amyloliquefaciens* dHJ9 in this study. Furthermore, degenerate strains might accumulate organic acids or other compounds that altered rhizosphere pH or micro-ecological balance, potentially exacerbating disease progression. For instance, seabuckthorn root exudates inhibited wolfberry (*Lycium barbarum*) growth by elevating rhizosphere soil pH

Table 3
Pot experiment biocontrol experiments.

Treatment	Disease index	Disease control effect (%)
Blank control group	16.67 ± 18.82a	——
Fusarium sp. F2 + water control group	58.33 ± 6.45b	——
Fusarium sp. F2 + CFS of strain *B. amyloliquefaciens* dHJ9	62.50 ± 17.68c	-7.14 ± 27.88c
Fusarium sp. F2 + bacterial suspension of strain *B. amyloliquefaciens* HJ9	41.67 ± 10.21d	28.57 ± 20.43d
Fusarium sp. F2 + CFS of strain *B. amyloliquefaciens* HJ9	18.75 ± 17.23e	67.86 ± 27.28e

Data are the mean ± standard error (n = 6). Different letters indicate a significant difference between treatment groups within each category as determined by an LSD test ($P < 0.05$).

and decreasing total carbon (Zhang et al., 2025). Alternatively, the degenerate strain *B. amyloliquefaciens* dHJ9 might secrete substances that were utilized by pathogens, for example, *Fusarium* species could utilize saponins as a carbon source (Wang et al., 2025a), potentially exacerbating disease. The observed aggravation of root rot by *B. amyloliquefaciens* dHJ9 in this study was contrary to the typical protective function of biocontrol agents. However, this was consistent with the earlier findings by Nicol et al. (2003) and Wang et al. (2025a), who reported that ginseng crude saponins could stimulate the growth of soil-borne pathogens. It is hypothesized that metabolic dysregulation in degenerate strains gives rise to similar outcomes. Our findings have important practical implications for quality control in the production of biological antifungal compounds. Therefore, it is essential to rigorously monitor metabolic stability throughout fermentation to prevent production-strain degeneration during subculturing.

3.4.10. Determination of IAA production

The capacity to synthesize plant growth-promoting substances is a key attribute of effective biocontrol agents for sustainable agriculture. The production of IAA, a crucial auxin, in both *B. amyloliquefaciens* HJ9 and its degenerate counterpart dHJ9, was quantified. As showed in Fig. 9, IAA yield of *B. amyloliquefaciens* HJ9 was significantly higher (38.77 ± 0.89 μg/mL) than that of its degenerate counterpart dHJ9 (11.92 ± 0.17 μg/mL). The results demonstrated that the degenerative process not only impaired the antibacterial and antifungal secondary metabolism, but also adversely affected the plant growth-promoting functions of the strain.

IAA is known to stimulate root development, enhance nutrient uptake, and improve overall plant vigor, thereby indirectly increasing host resistance to pathogens (Yuan et al., 2025). The ability of *B. amyloliquefaciens* HJ9 to produce substantial IAA highlighted its dual potential as both a biocontrol and a biofertilizer agent. The markedly reduced IAA production in *B. amyloliquefaciens* dHJ9 (Fig. 9) provided explained its inferior performance in pot experiments (Fig. 8), where it consequently failed to protect *P. cyrtonema* Hua seedlings. The loss of this growth-promoting trait compromised the ability of *B. amyloliquefaciens* dHJ9 to either directly inhibit the pathogen nor support the host plant's health and defense capacity. The degeneration highlights the necessity of maintaining strain stability during industrial-scale production and formulation. Effective quality control must therefore monitor both the integrity of antimicrobial gene clusters and the preservation of plant-beneficial traits to guarantee the reliability and efficacy of the final product.

3.4.11. Gene expression for lipopeptide antibiotic compounds

PCR analysis of the lipopeptide-associated genes *itu*A, *srf*AB, *bmy*A, and *bam*D was performed on both *B. amyloliquefaciens* HJ9 and its degenerate strain dHJ9 genomic DNA. All target genes were amplified as single bands in both strains, corresponding to the anticipated molecular weights. However, *Fen*B synthesis gene was not amplified (Fig. 10a and

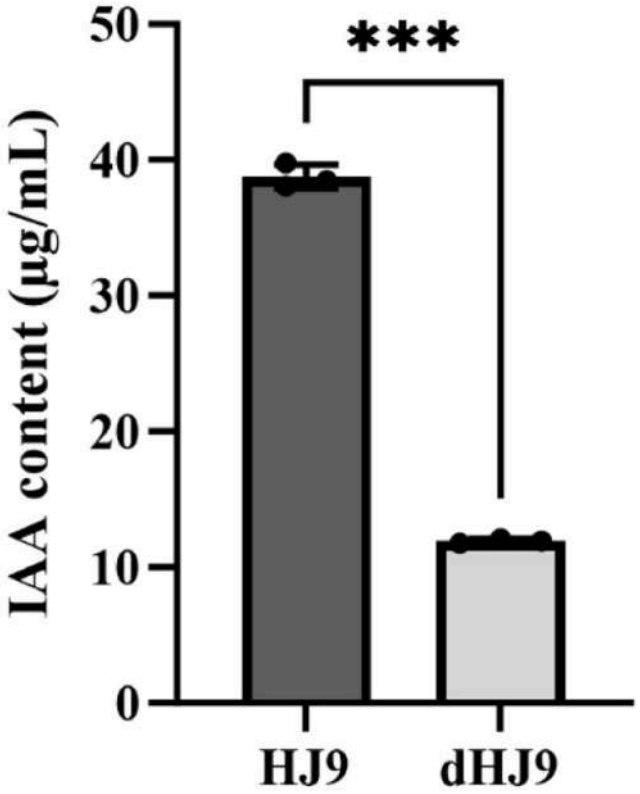

Fig. 9. IAA production by *B. amyloliquefaciens* HJ9 and its degenerate strain dHJ9. Different letters indicated significant differences ($p < 0.01$).

b). These results indicated that both *B. amyloliquefaciens* HJ9 and its degenerate strain dHJ9 were capable of producing lipopeptide antibiotics such as surfactin, iturin, bacillomycin D, and bacillaene. Compared to *B. amyloliquefaciens* HJ9, the degenerate strain dHJ9 showed significantly reduced expression of *itu*A (3.3-fold decrease, $p < 0.001$) and *bam*D (2.5-fold decrease, $p = 0.041$) genes. In contrast, the expression levels of *srf*AB and *bmy*A did not change significantly (Fig. 10c, d, e, f).

In the study by Wang et al. (2024), the antifungal activity of *Bacillus* strains was attributed primarily to iturin-family compounds, including iturin A. The normal expression of *Itu*A gene in *B. amyloliquefaciens* HJ9 enabled the synthesis of iturin, which possessed conserved antifungal activity shared by iturin A (Wang et al., 2024). In contrast, the expression of *Itu*A gene in the degenerate strain dHJ9 was downregulated by 3.3-fold, which might lead to reduced synthesis of iturin and consequently resulted in the complete loss of its inhibitory effect against *Fusarium* sp. F2 (Fig. 10). Xu (2014) reported that *bam*D gene encoded bacillomycin D synthetase, which was crucial for antifungal activity and biofilm formation in *B. amyloliquefaciens* SQR9. Knockout of *bam*D led to decreased antagonistic ability, delayed biofilm formation, and weakened rhizosphere colonization in the strain SQR9. The findings were consistent with the differential inhibition activity exhibited against *Fusarium* sp. F2 by *B. amyloliquefaciens* HJ9 compared to the degenerate strain dHJ9 in this study (Fig. 10). Therefore, the findings demonstrated that the reduced antifungal activity following degeneration was mainly attributable to alterations in gene expression regulation. Bacillaene and iturin were the key metabolites responsible for the inhibition of *Fusarium* sp. F2 by *B. amyloliquefaciens* HJ9. The downregulation of their biosynthetic genes directly led to reduced secretion of these compounds, thereby weakening antifungal effects such as disruption of pathogen cell membranes and induction of nucleic acid/protein leakage.

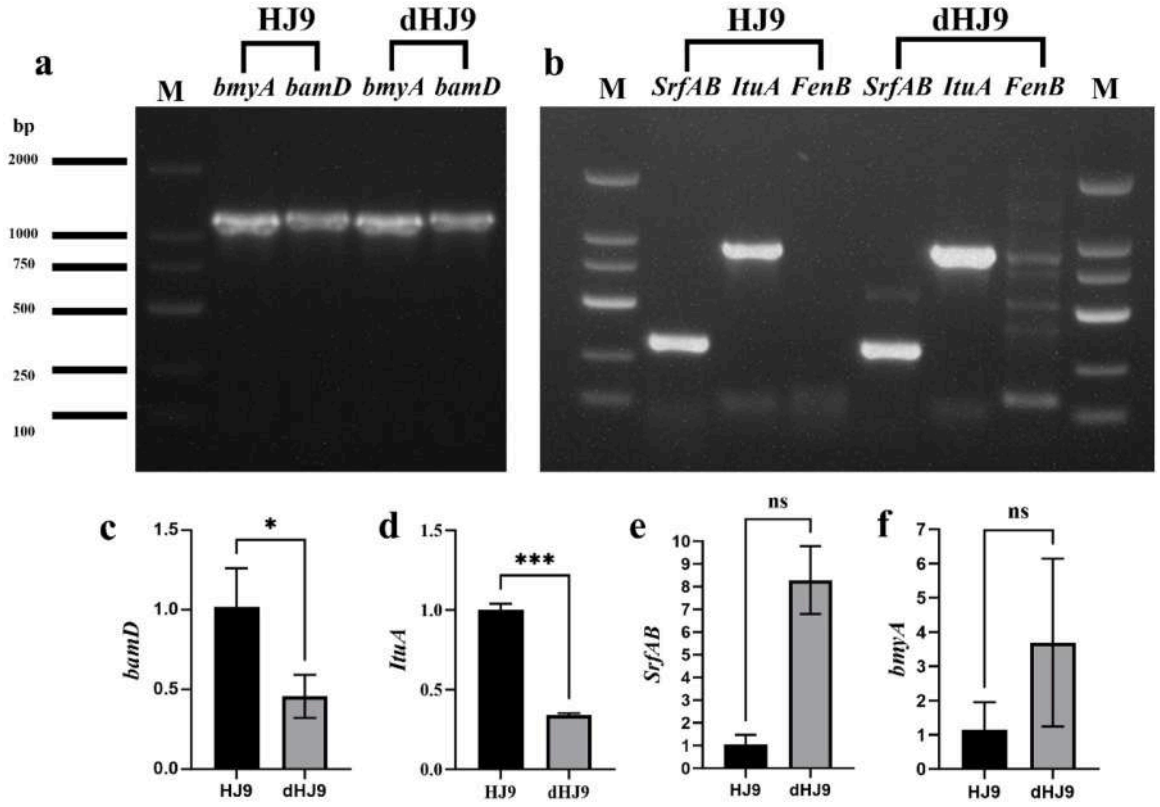

Fig. 10. Cloning and expression of genes related to lipopeptide antibiotic synthetases. a. Bacillomycin D *bmyA* gene and Bacillaene synthetase gene cluster *bamD* gene; b. Iturin A *ItuA*, Fengycin *FenB*, and Surfactin *SrfAB* genes; c. Expression differences of *bamD* gene between *B. amyloliquefaciens* HJ9 and its degenerate strain dHJ9; d. Expression differences of *ItuA* gene between *B. amyloliquefaciens* HJ9 and its degenerate strain dHJ9; e. Expression differences of *SrfAB* gene between *B. amyloliquefaciens* HJ9 and its degenerate strain dHJ9; f. Expression differences of *bmyA* gene between *B. amyloliquefaciens* HJ9 and its degenerate strain dHJ9.

4. Conclusions

In this work, 359 endophytic bacterial strains were successfully isolated from *P. cyrtonema* Hua, of which 56 exhibited significant antagonistic activity against common pathogens. Among the obtained endophytes, *B. amyloliquefaciens* HJ9, selected for its potent antimicrobial properties, demonstrated strong antagonism against *Fusarium* sp. F2. In contrast, its degenerate derivative, *B. amyloliquefaciens* dHJ9, exhibited a marked decline in antifungal activity. Mechanisms studies revealed that *B. amyloliquefaciens* HJ9 could inhibit the pathogen by secreting active metabolites that disrupted the integrity of the fungal cell membrane. This membrane damage led to the leakage of nucleic acids and proteins, enhanced PI staining, and elevated levels of membrane lipid peroxidation. Furthermore, *B. amyloliquefaciens* HJ9 CFS strongly suppressed spore germination and significantly inhibited early biofilm formation. However, the down-regulation of *ItuA* and *bamD* in *B. amyloliquefaciens* dHJ9 led to the absence of active metabolite synthesis, thereby failing to inhibit the fungal growth. In pot experiments, CFS of *B. amyloliquefaciens* HJ9 demonstrated the highest control efficacy, whereas *B. amyloliquefaciens* dHJ9 might accumulate pathogen-promoting substances due to metabolic dysregulation, resulting in an increased disease index. In addition to losing antifungal metabolites and key biosynthetic gene clusters, the degenerate strain *B. amyloliquefaciens* dHJ9 showed a pronounced reduction in the production of the plant growth hormone IAA.

In summary, *B. amyloliquefaciens* HJ9 considered as a biocontrol agent, were primarily by targeting and disrupting the pathogen cell membrane and inhibiting biofilm formation. The loss of activity in the degenerate strain *B. amyloliquefaciens* dHJ9 was mainly due to the dysregulation of its secondary metabolic pathways. This study provided a theoretical basis for developing stable biocontrol formulations based on the active metabolites of *B. amyloliquefaciens* HJ9. In future studies, the focus should be on the expression regulation mechanisms of lipopeptide synthesis gene clusters to construct degeneration-resistant engineered strains. Furthermore, a deeper investigation into the molecular basis of the strong antagonistic activity of *B. amyloliquefaciens* HJ9, as well as the mechanisms underlying functional loss in the degenerate strain *B. amyloliquefaciens* dHJ9, is also carried out.

CRediT authorship contribution statement

Yan-Xi Chen: Investigation, Data curation. **Zhen-Xing Tang:** Writing – review & editing. **Yue Fu:** Investigation, Formal analysis. **Lu-E Shi:** Writing – review & editing, Supervision, Conceptualization. **Er-Xu Pi:** Writing – review & editing, Resources. **Zi-Xin Wang:** Investigation, Data curation. **Xin-Pei Ye:** Writing – original draft, Investigation. **Yu-Hang Zhou:** Resources, Project administration. **Shu-Qi Chen:** Investigation, Formal analysis. **Yu-Huan Wu:** Writing – review & editing. **Shu-Jie Lin:** Formal analysis, Data curation.

Declaration of Competing Interest

The authors declare that they have no known competing financial interests or personal relationships that could have appeared to influence the work reported in this paper.

Acknowledgement

This research was funded by the projects of Teaching Reform program of the '14th Five-Year Plan' of Zhejiang Higher Vocational Education (No. jg20240094).

Data availability

Data will be made available on request.

References

Acosta-González, U., Silva-Rojas, H.V., Fuentes-Aragón, D., Hernández-Castrejón, J., Romero-Bautista, A., Rebollar-Alviter, A., 2022. Comparative performance of fungicides and biocontrol products in the management of fusarium wilt of blackberry. Plant Dis. 106 (5), 1419–1427. https://doi.org/10.1094/pdis-08-21-1742-re.

Aflakian, F., Hashemitabar, G., 2025. Biosynthesized silver nanoparticles at subinhibitory concentrations as inhibitors of quorum sensing, pathogenicity, and biofilm formation in *Pseudomonas aeruginosa* PAO1. Heliyon 11 (4), e42899. https://doi.org/10.1016/j.heliyon.2025.e42899.

Aydin, M.H., 2019. Evaluation of some *Trichoderma* species in biological control of potato dry rot caused by *Fusarium sambucinum* fuckel isolates. Appl. Ecol. Environ. Res. 17 (1), 533–546. https://doi.org/10.15666/aeer/1701_533546.

Bedine, M.A.B., Ntsoli, P.G., Moussango, V.D., Beyegue, H.D., Yaouba, A., Tchameni, S. N., Sameza, M.L., 2025. Assessing the effectiveness of plant extracts for mitigating physicochemical alterations mediated by *Fusarium* spp. on potato tubers. Postharvest Biol. Technol. 230, 113736. https://doi.org/10.1016/j.postharvbio.2025.113736.

Botsoglou, N.A., Fletouris, D.J., Papageorgiou, G.E., Vassilopoulos, V.N., Mantis, A.J., Trakatellis, A.G., 1994. Rapid, sensitive, and specific thiobarbituric acid method for measuring lipid peroxidation in animal tissue, food, and feedstuff samples. J. Agric. Food Chem. 42 (9), 1931–1937. https://doi.org/10.1021/jf00045a019.

Bui, P.H., Pham, D.-P., Nguyen, T.-V., Nguyen, T.-H., Le-Nguyen, N.-T., Le Vo, T.D., Huynh-Ngoc, T.-D., Tran, T.-T., Huynh, T., 2025. Genomic features of plant growth-promoting Ochrobactrum intermedium GH3, an endophyte associated with flatsedge (Cyperus sp.) native to Hochiminh City, Vietnam. World J. Microbiol. Biotechnol. 41 (8), 281. https://doi.org/10.1007/s11274-025-04502-8.

Chaudhary, P., Agri, U., Chaudhary, A., Kumar, A., Kumar, G., 2022. Endophytes and their potential in biotic stress management and crop production. Front. Microbiol 13, 933017. https://doi.org/10.3389/fmicb.2022.933017.

Chen, X., Gu, Q., Chu, B., Zhang, Y., Chen, Z., Ma, M., Li, D., Lu, J., Wu, D., 2024. Inhibition mechanism of *fusarium* graminearum growth by g-C(3)N(4) homojunction and its application in barley malting. Int. J. Food Microbiol 413, 110578. https://doi.org/10.1016/j.ijfoodmicro.2024.110578.

Chen, X.H., Koumoutsi, A., Scholz, R., Eisenreich, A., Schneider, K., Heinemeyer, I., Morgenstern, B., Voss, B., Hess, W.R., Reva, O., Junge, H., Voigt, B., Jungblut, P.R., Vater, J., Süssmuth, R., Liesegang, H., Strittmatter, A., Gottschalk, G., Borriss, R., 2007. Comparative analysis of the complete genome sequence of the plant growth–promoting bacterium *Bacillus amyloliquefaciens* FZB42. Nat. Biotechnol. 25 (9), 1007–1014. https://doi.org/10.1038/nbt1325.

Cheng, Y., Lou, H., He, H., He, X., Wang, Z., Gao, X., Liu, J., 2024. Genomic and biological control of Sclerotinia sclerotiorum using an extracellular extract from *Bacillus velezensis* 20507. Front. Microbiol. 15, 1385067. https://doi.org/10.3389/fmicb.2024.1385067.

Chi, H., Zhuang, Y., Zeng, X., Chen, W., Mao, B., 2019. Isolation and identification of antagonistic endophytic *Bacillus velezensisfrom Polygonatum cyrtonema* Hua and analysis of itsantimicrobial and growth-promoting activity. Plant Prot. 45 (04), 122–131. https://doi.org/10.16688/j.zwbh.2018337.

Coico, R., 2005. Gram staining. Curr. Protoc. Microbiol. Append. 3 Append. 3C. https://doi.org/10.1002/9780471729259.mca03cs00.

Du, T.Y., Karunarathna, S.C., Zhang, X., Dai, D.Q., Mapook, A., Suwannarach, N., Xu, J. C., Stephenson, S.L., Elgorban, A.M., Al-Rejaie, S., Tibpromma, S., 2022. Endophytic fungi associated with *Aquilaria sinensis (Agarwood)* from China show antagonism against bacterial and fungal pathogens. J. Fungi 8 (11), 1197. https://doi.org/10.3390/jof8111197.

Ezzat, A., Szabó, S., Szabó, Z., Hegedűs, A., Berényi, D., Holb, I.J., 2021. Temporal patterns and inter-correlations among physical and antioxidant attributes and enzyme activities of apricot fruit inoculated with *Monilinia laxa* under salicylic acid and methyl jasmonate treatments under shelf-life conditions. J. Fungi 7 (5), 341. https://doi.org/10.3390/jof7050341.

Feng, J., Fan, Z., Zheng, L., Chen, Z., Liu, C., Wang, H., Peng, X., Chen, F., 2025. Study on the growth inhibition and mechanism of *Bacillus Subtilis* B579 metabolites on *Fusarium Oxysporum*. J. Liaocheng Univ. (Nat. Sci. Ed.) 1–8. https://doi.org/10.19728/j.issn1672-6634.2025010007.

Franco, M.E.E., Nickerson, M.N., Bowen, B.P., Louie, K., Northen, T.R., U'Ren, J.M., 2025. Hyperdiverse, bioactive, and interaction-specific metabolites produced only in co-culture suggest diverse competitors may fuel secondary metabolism of xylarialean fungi. mSystems 10 (7), e00468-25. https://doi.org/10.1128/msystems.00468-25.

Gonzalez, M.F., Magdama, F., Galarza, L., Sosa, D., Romero, C., 2020. Evaluation of the sensitivity and synergistic effect of Trichoderma reesei and mancozeb to inhibit under in vitro conditions the growth of *Fusarium oxysporum*. Commun. Integr. Biol. 13 (1), 160–169. https://doi.org/10.1080/19420889.2020.1829267.

Han, Z., Gong, Q., Huang, S., Meng, X., Xu, Y., Li, L., Shi, Y., Lin, J., Chen, X., Li, C., Ma, H., Liu, J., Zhang, X., Chen, D., Si, J., 2023. Machine learning uncovers accumulation mechanism of flavonoid compounds in *Polygonatum cyrtonema* Hua. Plant Physiol. Biochem 201, 107839. https://doi.org/10.1016/j.plaphy.2023.107839.

Han, F., Li, Q., Han, R., Zhang, W., Yu, Z., Lin, M., Yang, J., 2020. Isolation and identification of pathogen of *Polygonatum cyrtonema Hua* root rot disease in Chongqing. Mol. Plant Breed. 18 (11), 3693–3698. https://doi.org/10.13271/j.mpb.018.003693.

Hari, A., Lahlali, R., Ortaakarsu, A.B., Taarji, N., Laasli, S.-E., Karaaoui, K., Benjelloun, M., Ouchari, W., Sobeh, M., Echchgadda, G., 2024. Inhibitory effects of wild Origanum elongatum extracts on *Fusarium oxysporum* mycelium growth and spores germination: evidence from in-vitro, in-planta, and in-silico experiments. J. Nat. Pestic. Res. 10, 100096. https://doi.org/10.1016/j.napere.2024.100096.

He, J., Dong, J., Zhang, W., Cheng, Y., Xie, J., Ji, X., Ullah, F., Ma, Y., Kong, W., 2025. Comparative unravelling the antifungal activity and mechanism of oleuropein and matrine inhibiting the growth of phytopathogen *Fusarium* spp. Pestic. Biochem. Physiol. 213, 106538. https://doi.org/10.1016/j.pestbp.2025.106538.

He, Y., Huang, L., Jiang, P., Xu, G., Sun, T., 2022. Immunological regulation of the active fraction from *Polygonatum sibiricum F. Delaroche* based on improvement of intestinal microflora and activation of RAW264.7 cells. J. Ethnopharmacol. 293, 115240. https://doi.org/10.1016/j.jep.2022.115240.

He, J., Lei, B., Song, Z., Geng, K., Kang, J., 2014. Determination of the inhibitory effect of endophyte DEB-2 on five pepper fungal pathogens in the laboratory. Acta Phytophy. Sin. 41 (02), 157–162. https://doi.org/10.13802/j.cnki.zwbhxb.2014.02.006.

Huang, L., Wu, Y., Yin, H., Yang, X., Yuan, M., Ning, H., 2021. Two new compounds from the stewed *Polygonatum cyrtonema* Hua and their protective effect against Aβ(25-35) induced cytotoxicity and oxidative stress damage. Nat. Prod. Res. 35 (23), 4945–4952. https://doi.org/10.1080/14786419.2020.1753735.

Huang, X., Zheng, M., Yi, Y., Patel, A., Song, Z., Li, Y., 2020. Inhibition of berberine hydrochloride on *Candida albicans* biofilm formation. Biotechnol. Lett. 42 (11), 2263–2269. https://doi.org/10.1007/s10529-020-02938-6.

Jamali, H., Sharma, A., Kushwaha, P., Kashyap, P., Srivastava, A., 2018. Exploitation of multifarious abiotic stresses, antagonistic activity and plant growth promoting attributes of *Bacillus amyloliquefaciens* AH53 for sustainable agriculture production. Int. J. Curr. Microbiol. Appl. Sci. 7, 751–763. https://doi.org/10.20546/ijcmas.2018.710.083.

Jiao, W., Liu, X., Chen, Q., Du, Y., Li, Y., Yue, F., Dong, X., Fu, M., 2020. Epsilon-poly-l-lysine (ε-PL) exhibits antifungal activity in vivo and in vitro against *Botrytis cinerea* and mechanism involved. Postharvest Biol. Technol. 168, 111270. https://doi.org/10.1016/j.postharvbio.2020.111270.

Kadam, K.L., Wollweber, K.L., Grosch, J.C., Jao, Y.C., 1987. Investigation of plasmid instability in amylase-producing *B. subtilis* using continuous culture. Biotechnol. Bioeng. 29 (7), 859–872. https://doi.org/10.1002/bit.260290708.

Kaye, E., Nyombi, A., Mutambuze, I.L., Muwesa, R., 2015. Mancozeb residue on tomatoes in central Uganda. J. Health Pollut. 5 (8), 1–6. https://doi.org/10.5696/i2156-9614-5-8.1.

Khan, H., Saeed, M., Muhammad, N., Ghaffar, R., Khan, S.A., Hassan, S., 2012. Antimicrobial activities of rhizomes of *Polygonatum verticillatum*: attributed to its total flavonoidal and phenolic contents. Pak. J. Pharm. Sci. 25 (2), 463–467.

Li, B., He, X., Guo, S., Li, D., Wang, Y., Meng, X., Dai, P., Hu, T., Cao, K., Wang, S., 2024. Characterization of *Bacillus amyloliquefaciens* BA-4 and its biocontrol potential against *Fusarium*-related apple replant disease. Front. Plant Sci. 15, 1370440. https://doi.org/10.3389/fpls.2024.1370440.

Liang, Z., Li, J., 2021. Isolation and identification of the pathogenic fungi of *Polygonatum cyrtonema Hua* root rot in Hunan Province. J. South. Agric. 52 (07), 1923–1930. https://doi.org/10.3969/j.issn.2095-1191.2021.07.022.

Lin, S., Li, X., Zhang, W., Shu, G., Tolker-Nielsen, T., Li, H., Xu, F., Lin, J., Peng, G., Zhang, L., Fu, H., 2025. Enhanced penetration and biofilm eradication by sophorolipid micelles encapsulating Honokiol: a comprehensive solution for biofilm-associated lung infections. J. Nanobiotechnol. 23, 76. https://doi.org/10.1186/s12951-025-03144-0.

Liu, H., Cheng, H., Xu, J., Hu, J., Zhao, C., Xing, L., Wang, M., Wu, Z., Peng, D., Yu, N., Liu, J., 2023. Genetic diversity and population structure of *Polygonatum cyrtonema* Hua in China using SSR markers. PLoS One 18 (8), e0290605. https://doi.org/10.1371/journal.pone.0290605.

Liu, G., Feng, S., Sui, M., Chen, B., Sun, P., 2023. Extraction and identification of steroidal saponins from *Polygonatum cyrtonema Hua* using natural deep eutectic solvent-synergistic quartz sand-assisted extraction method. J. Sep. Sci. 46 (7), e2200823. https://doi.org/10.1002/jssc.202200823.

Liu, S., Fu, L., Wang, S., Chen, J., Jiang, J., Che, Z., Tian, Y., Chen, G., 2019. Carbendazim resistance of *Fusarium graminearum* from Henan wheat. Plant Dis. 103 (10), 2536–2540. https://doi.org/10.1094/pdis-02-19-0391-re.

Liu, F., Yang, S., Xu, F., Zhang, Z., Lu, Y., Zhang, J., Wang, G., 2022. Characteristics of biological control and mechanisms of *Pseudomonas chlororaphis* zm-1 against peanut stem rot. BMC Microbiol. 22 (1), 9. https://doi.org/10.1186/s12866-021-02420-x.

Liu, R., Zhang, X., Cai, Y., Xu, S., Xu, Q., Ling, C., Li, X., Li, W., Liu, P., Liu, W., 2024. Research progress on medicinal components and pharmacological activities of *polygonatum sibiricum*. J. Ethnopharmacol. 328, 118024. https://doi.org/10.1016/j.jep.2024.118024.

Long, T., Liu, Z., Shang, J., Zhou, X., Yu, S., Tian, H., Bao, Y., 2018. *Polygonatum sibiricum* polysaccharides play anti-cancer effect through TLR4-MAPK/NF-κB signaling pathways. Int. J. Biol. Macromol. 111, 813–821. https://doi.org/10.1016/j.ijbiomac.2018.01.070.

Lu, S., Xiao, B., Ren, F., Zhuo, W., Huang, H., 2021. Fungal community structure and diversity of rhizosphere soil of *Polygonatum Sibiricum* with root-rot analyzed by Illumina MiSeq high-throughput sequencing technology. World Sci. Technol. Mod. Tradit. Chin. Med. 23 (01), 13–19. ⟨https://link.cnki.net/urlid/11.5699.r.20210304.1401.014⟩.

Luo, L., Zhao, C., Wang, E., Raza, A., Yin, C., 2022. *Bacillus amyloliquefaciens* as an excellent agent for biofertilizer and biocontrol in agriculture: an overview for its mechanisms. Microbiol. Res. 259, 127016. https://doi.org/10.1016/j.micres.2022.127016.

Lyu, C., Xia, J., Lin, Y., Liu, X., Xiang, A., Zheng, Y., Bai, X., 2022. Identification and antimicrobial activity of an antagonistic endophyticstrain HJ-3 from *Polygonatum cyrtonema*. Nat. Prod. Res. Dev. 34 (03), 399–406. https://doi.org/10.16333/j.1001-6880.2022.3.006.

Ma, Y., Wu, M., Qin, X., Dong, Q., Li, Z., 2023. Antimicrobial function of yeast against pathogenic and spoilage microorganisms via either antagonism or encapsulation: a review. Food Microbiol. 112, 104242. https://doi.org/10.1016/j.fm.2023.104242.

Mao, Z., Zhang, W., Wu, C., Feng, H., Peng, Y., Shahid, H., Cui, Z., Ding, P., Shan, T., 2021. Diversity and antibacterial activity of fungal endophytes from *Eucalyptus exserta*. BMC Microbiol. 21 (1), 155. https://doi.org/10.1186/s12866-021-02229-8.

Meng, X., Wu, W., Niu, B., Liu, R., Chen, H., Gao, H., Chen, H., 2024. Inhibitory effect and action mechanism of perillaldehyde on the *Fusarium graminearum* in postharvest fresh ginger. Postharvest Biol. Technol. 209, 112674. https://doi.org/10.1016/j.postharvbio.2023.112674.

Mohan, A., Matthews, B., Räsänen, K., 2024. Direct and indirect effects of chemical pollution: fungicides alter growth, feeding, and pigmentation of the freshwater detritivore Asellus aquaticus. Ecotoxicol. Environ. Saf. 285, 117017. https://doi.org/10.1016/j.ecoenv.2024.117017.

Negi, R., Sharma, B., Kumar, S., Chaubey, K.K., Kaur, T., Devi, R., Yadav, A., Kour, D., Yadav, A.N., 2024. Plant endophytes: Unveiling hidden applications toward agro-environment sustainability. Folia Parasitol. 69 (1), 181–206. https://doi.org/10.1007/s12223-023-01092-6.

Nicol, R.W., Yousef, L., Traquair, J.A., Bernards, M.A., 2003. Ginsenosides stimulate the growth of soilborne pathogens of American ginseng. Phytochemistry 64 (1), 257–264. https://doi.org/10.1016/S0031-9422(03)00271-1.

Palmieri, D., Vitale, S., Lima, G., Di Pietro, A., Turrà, D., 2020. A bacterial endophyte exploits chemotropism of a fungal pathogen for plant colonization. Nat. Commun. 11 (1), 5264. https://doi.org/10.1038/s41467-020-18994-5.

Pan, C., Ye, Y., Ma, Y., Li, S., Zhu, Y., Chu, Y., Wang, F., Shen, L., Tian, J., 2025. Cinnamaldehyde triggers fungal apoptosis in *Fusarium solani* by impairing cell structures and antioxidant defense through restricting glucose availability. Food Biosci. 69, 106889. https://doi.org/10.1016/j.fbio.2025.106889.

Pandey, S.S., Jain, R., Bhardwaj, P., Thakur, A., Kumari, M., Bhushan, S., Kumar, S., 2022. Plant probiotics - Endophytes pivotal to plant health. Microbiol. Res. 263, 127148. https://doi.org/10.1016/j.micres.2022.127148.

Pang, Z., Mao, X., Xia, Y., Xiao, J., Wang, X., Xu, P., Liu, G., 2022. Multiomics reveals the effect of root rot on *Polygonati Rhizome* and identifies pathogens and biocontrol strain. Microbiol. Spectr. 10 (2), e0238521. https://doi.org/10.1128/spectrum.02385-21.

Peng, Y., Fang, J., Wu, Z., Liao, K., Guo, P., 2024. The effect of andrographolide on the biofilm formation and adhesion ability of *Fusarium keratoplasticum*. Chin. J. Mycol. 19 (02), 113–116. +137.

Pereira, R., Dos Santos Fontenelle, R.O., de Brito, E.H.S., de Morais, S.M., 2021. Biofilm of *Candida albicans*: formation, regulation and resistance. J. Appl. Microbiol 131 (1), 11–22. https://doi.org/10.1111/jam.14949.

Ren, J., Cao, T., Zang, X., Liu, J., Yang, D., 2024. Antifungal mechanisms and characteristics of *Pseudomonas fluorescens*: promoting peanut growth and combating *Fusarium oxysporum*-induced root rot. Plant Physiol. Biochem 216, 109092. https://doi.org/10.1016/j.plaphy.2024.109092.

Ren, S., Liu, L., Chang, L., Li, J., Liu, G., 2017. Degeneration and control of adenosine high-yielding strains of *Bacillus subtilis* DI4-24. Ind. Microbiol 47 (02), 24–28.

Ribeiro, C.M., Cardoso, E.J.B.N., 2012. Isolation, selection and characterization of root-associated growth promoting bacteria in *Brazil Pine* (Araucaria angustifolia). Microbiol. Res. 167, 69–78. https://doi.org/10.1016/j.micres.2011.03.003.

Sahu, P.K., Tilgam, J., Mishra, S., Hamid, S., Gupta, A., K, J., Verma, S.K., Kharwar, R.N., 2022. Surface sterilization for isolation of endophytes: ensuring what (not) to grow. J. Basic Microbiol 62 (6), 647–668. https://doi.org/10.1002/jobm.202100462.

Saikia, B., Bhattacharyya, A., Chandra Boro, R., Savani, A.K., V, B., 2025. Bioprospecting of bacterial endophytes from Solanum pimpinellifolium with antifungal activity against Fusarium oxysporum f.sp. lycopersici causing vascular wilt. Physiol. Mol. Plant Pathol. 136, 102566. https://doi.org/10.1016/j.pmpp.2025.102566.

Sav, H., Rafati, H., Öz, Y., Dalyan-Cilo, B., Ener, B., Mohammadi, F., Ilkit, M., van Diepeningen, A.D., Seyedmousavi, S., 2018. Biofilm formation and resistance to fungicides in clinically relevant members of the fungal genus *Fusarium*. J. Fungi 4 (1), 16. https://doi.org/10.3390/jof4010016.

Sha, Y., Zeng, Q., Tian, X., Li, Y., Xu, J., 2025. Screening and control effect of *Bacillus* on root rot of Chinese herbal medicines. Chin. J. Biol. Control 41 (03), 520–529. https://doi.org/10.16409/j.cnki.2095-039x.2025.02.025.

Sharma, H., Fidan, H., Özogul, F., Rocha, J.M., 2022. Recent development in the preservation effect of *lactic acid bacteria* and essential oils on chicken and seafood products. Front. Microbiol 13, 1092248. https://doi.org/10.3389/fmicb.2022.1092248.

Shay, R., Wiegand, A.A., Trail, F., 2022. Biofilm formation and structure in the filamentous fungus *Fusarium graminearum*, a plant pathogen. Microbiol. Spectr. 10 (4), e0017122. https://doi.org/10.1128/spectrum.00171-22.

Shi, J.Y., Wang, Y.J., Bao, Q.W., Qin, Y.M., Li, P.P., Wu, Q.Q., Xia, C.K., Wu, D.L., Xie, S. Z., 2025. *Polygonatum cyrtonema* Hua polysaccharide alleviates ulcerative colitis via gut microbiota-independent modulation of inflammatory immune response. Carbohydr. Polym. 356, 123387. https://doi.org/10.1016/j.carbpol.2025.123387.

Sun, L., Deng, G.L., Wu, H.L., He, Q., Hu, S.H., Li, J.Y., Li, X.Y., Meng, S., He, A.N., Tian, Y.Q., Chen, X., Li, S.H., 2025. Biocontrol of gray spot disease on *Polygonatum cyrtonema* Hua by Bacillus velezensis GX1. Biol. Control 201, 105704. https://doi.org/10.1016/j.biocontrol.2025.105704.

Sun, Q., Li, J., Sun, Y., Chen, Q., Zhang, L., Le, T., 2020. The antifungal effects of cinnamaldehyde against *Aspergillus niger* and its application in bread preservation. Food Chem. 317, 126405. https://doi.org/10.1016/j.foodchem.2020.126405.

Tang, H., Dai, Y., Fu, Y., Zou, Y., Gao, Z., Pan, S., Wang, W., Yang, J., Bian, X., 2024. Inhibitory mechanism of bacilosarcin B from *Bacillus subtilis* against *Photobacterium damselae*. Microbiol. China 51 (02), 419–432. https://doi.org/10.13344/j.microbiol.china.230732.

Tang, X., Tang, Y., Li, Z., 1996. Strain degeneration of *Beauveria Bassiana* and its effecton control of *Pine Caterpillar*, *Dendrolimus Punctatus*. J. Anhui Agric. Univ. 03, 246–253.

Tiwari, R.K., Kumar, R., Sharma, S., Sagar, V., Aggarwal, R., Naga, K.C., Lal, M.K., Chourasia, K.N., Kumar, D., Kumar, M., 2020. Potato dry rot disease: current status, pathogenomics and management. 3 Biotech 10 (11), 503. https://doi.org/10.1007/s13205-020-02496-8.

Urooj, F., Farhat, H., 2025. Induction of endophytic fungi and algae regulates gene expression profiling in sunflower. S. Afr. J. Bot. 184, 1141–1148. https://doi.org/10.1016/j.sajb.2025.07.012.

Wang, Y., Chen, S., Chen, Y., Jin, C., Yan, J., Zhu, X., Guo, K., 2025. Identification and pathogenicity determination of the pathogen of *Polygonatum Cyrtonema* Root Rot in Xinhua. Mol. Plant Breed. 1–8. ⟨https://link.cnki.net/urlid/46.1068.S.20250520.1527.006⟩.

Wang, X., Peng, Y., Song, Y., Hua, J., Luo, S., 2025. Rhizospheric ginsenosides released from roots infected with root rot improve infectivity of pathogenic *Fusarium* fungi in ginseng. Physiol. Mol. Plant Pathol. 139, 102780. https://doi.org/10.1016/j.pmpp.2025.102780.

Wang, F., Wei, G., Zhao, W., Wang, H., Li, Z., Qiu, H., Hu, A., 2023. Identification of pathogen causing root rot in *Polygonatum cyrtonema Hua* and screening of biocontrol bacterias. Guangdong Agric. Sci. 50 (08), 143–153. https://doi.org/10.16768/j.issn.1004-874X.2023.08.015.

Wang, S., Xu, M., Han, Y., Zhou, Z., 2024. Exploring mechanisms of antifungal lipopeptide Iturin A from *Bacillus* against *Aspergillus niger*. J. Fungi 10, 172. https://doi.org/10.3390/jof10030172.

Wang, Y., Zhang, J., Sun, J., Li, G., Wang, Q., Zhao, Y., Ma, C., Han, J., 2023. Insights into the mechanisms of microbiome and metabolome changes mediated by understory interplanting mode in *Polygonatum sibiricum*. Front. Microbiol 17, 1218595. https://doi.org/10.3389/fmicb.2023.1232846.

Wu, F., Wang, H., Lin, Y., Feng, S., Li, X., 2025. Biocontrol mechanisms of antagonistic yeasts on postharvest fruits and vegetables and the approaches to enhance the biocontrol potential of antagonistic yeasts. Int. J. Food Microbiol. 430, 111038. https://doi.org/10.1016/j.ijfoodmicro.2024.111038.

Wu, Z., Zhong, M., Lu, C., Liu, P., Zhan, Z., Shao, K., Li, K., 2018. Effects of the crude extract from *Streptomyces* sp . N2 on cell membrane and antioxidant function of *Rhizoctonia solani*. J. Nucl. Agric. Sci. 32 (04), 700–707. https://doi.org/10.11869/j.issn.100-8551.2018.04.0700.

Wu, Y., Zhou, J., Li, C., Ma, Y., 2019. Antifungal and plant growth promotion activity of volatile organic compounds produced by *Bacillus amyloliquefaciens*. Microbiologyopen 8 (8), e00813. https://doi.org/10.1002/mbo3.813.

Xu, M., Shi, Y., Fan, D.L., Kang, Y.J., Yan, X.L., Wang, H.W., 2023. Co-culture of white rot fungi *Pleurotus ostreatus* P5 and *Bacillus amyloliquefaciens* B2: a strategy to enhance lipopeptide production and suppress of fusarium wilt of cucumber. J. Fungi 9 (11), 1049. https://doi.org/10.3390/jof9111049.

Xu, J., Tang, C., Din, A.U., Lu, Y., Ma, X., Zhang, T., Wu, J., Zuoqin, D., Luo, P., Wu, J., 2023. Oligosaccharides of *Polygonatum Cyrtonema* Hua ameliorates dextran sulfate sodium-induced colitis and regulates the gut microbiota. Biomed. Pharm. 161, 114562. https://doi.org/10.1016/j.biopha.2023.114562.

Xu Z., 2014. The molecular mechanisms of biofilm formation and cucumber root colonization of Bacillus amyloliouefaciens SOR9. Nanjing Agricultural University.

Xue, H., Bi, Y., Prusky, D., Raza, H., Zhang, R., Zhang, S., Nan, M., Zong, Y., Cheng, X., 2019. The mechanism of induced resistance against *Fusarium* dry rot in potato tubers by the T-2 toxin. Postharvest Biol. Technol. 153, 69–78. https://doi.org/10.1016/j.postharvbio.2019.03.021.

Yan, H., Meng, X., Lin, X., Duan, N., Wang, Z., Wu, S., 2023. Antifungal activity and inhibitory mechanisms of ferulic acid against the growth of *Fusarium graminearum*. Food Biosci. 52, 102414. https://doi.org/10.1016/j.fbio.2023.102414.

Yang, R., Shi, H., Lang, J., Lu, N., 2024. The antibacterial mechanism of *Bacillus amyloliquefaciens* PB-1 against *Botrytis cinerea*. Jiangsu Agric. Sci. 52, 149–155. https://doi.org/10.15889/j.issn.1002-1302.2024.16.019.

Yang, L., Zeng, N., Huang, P., Shu, G., 2025. Study on *in vitro* antibacterial activity and mechanism of Yinhuang soluble powder against drug - resistant *Streptococcus suis*. Chin. J. Vet. Drug 59 (05), 29–38. https://doi.org/10.11751/ISSN.1002-1280.2025.5.05.

Yang, J.J., Zhang, X., Dai, J.F., Ma, Y.G., Jiang, J.G., 2023. Effect of fermentation modification on the physicochemical characteristics and anti-aging related activities of *Polygonatum kingianum* polysaccharides. Int. J. Biol. Macromol. 235, 123661. https://doi.org/10.1016/j.ijbiomac.2023.123661.

Yi, Y., Luan, P., Fan, M., Wu, X., Sun, Z., Shang, Z., Yang, Y., Li, C., 2024. Antifungal efficacy of *Bacillus amyloliquefaciens* ZK-9 against *Fusarium graminearum* and analysis of the potential mechanism of its lipopeptides. Int. J. Food Microbiol. 422, 110821. https://doi.org/10.1016/j.ijfoodmicro.2024.110821.

Yi, L., Yang, M., Waalwijk, C., Xu, J., Xu, J., Molnár, O., Chen, W., Feng, J., Zhang, H., 2023. Dynamics of carbendazim-resistance frequency of pathogens associated with the epidemic of fusarium head blight. Plant Dis. 107 (6), 1690–1696. https://doi.org/10.1094/pdis-08-22-1998-sr.

Yuan, Q.S., Luo, L., Shi, H., Wang, H., An, J., Gao, Y., Xu, J., Ou, X., Yang, Y., Tabl, K.M., Guo, L., Huang, L., Zhou, T., 2025. Fungal symbiont *Mycena* complements impaired nitrogen utilization in *Gastrodia elata* and supplies indole-3-acetic acid to facilitate its seed germination. Plant Commun. 6, 101500. https://doi.org/10.1016/j.xplc.2025.101500.

Zeng, T., Tang, Y.R., Li, B., Tasneem, S., Yuan, H.W., Jia, Y.Z., Daniyal, M., Hussain, N., Wang, W.M., Zuo, D.L., Gong, L.M., Liu, B., Shi, J.L., Zhou, Z., Peng, C.Y., He, S.J.,

Wang, W., 2020. Chemical characterization of constituents from *Polygonatum cyrtonema* Hua and their cytotoxic and antioxidant evaluation. Nat. Prod. Res. 34 (17), 2482–2489. https://doi.org/10.1080/14786419.2018.1543682.

Zeng, K., Zhao, Z., Li, Y., Qi, K., Xu, W., Zha, L., 2025. Screening and whole-genome analysis of Indole-3-acetic acid-producing endophytic bacterium ALX01 from *Atractylodes lancea*. Mod. Chin. Med. 27, 1750–1758. https://doi.org/10.13313/j.issn.1673-4890.20250422002.

Zhai, D., Fang, Z., Lv, C., Zhang, M., Liu, S., Wu, M., Fang, R., Zhou, X., Fang, J., Bai, X., 2019. Research on antibacterial activity of the endophytic *Bacillus subtilis* HJ-2 from *Polygonatum cyrtonema*. J. Agric. Biotechnol. 27 (09), 1664–1672. https://doi.org/10.3969/j.issn.1674-7968.2019.09.015.

Zhang, M., Li, X., Pan, Y., Qi, D., Zhou, D., Chen, Y., Feng, J., Wei, Y., Zhao, Y., Li, K., Wang, W., Zhang, L., Xie, J., 2024. Biocontrol mechanism of Bacillus siamensis sp. QN2MO-1 against tomato fusarium wilt disease during fruit postharvest and planting. Microbiol. Res. 283, 127694. https://doi.org/10.1016/j.micres.2024.127694.

Zhang, R., Qu, S., Zhang, B., Gao, Y., Xing, F., 2025. The response mechanism of high-quality grass to typical poisonous weed root exudates and litter: using *Leymus chinensis* and *Stellera chamaejasme* as examples. Appl. Soil Ecol. 206, 105858. https://doi.org/10.1016/j.apsoil.2024.105858.

Zhang, Y., Wang, Y., Zhao, X., Liu, L., Xing, R., Song, X., Zou, Y., Li, L., Wan, H., Jia, R., Yin, L., Liang, X., He, C., Wei, Q., Yin, Z., 2022. Study on the anti-biofilm mechanism of 1,8-cineole against *Fusarium solani* species complex. Front. Pharm. 13, 1010593. https://doi.org/10.3389/fphar.2022.1010593.

Zhang, T., Wu, D., Ma, J., Chen, J., Fang, Y., Chen, B., Wei, T., 2023. Establishment of the *Cordyceps militaris* degeneration gradient and variations in related molecular mechanisms. Mod. Food Sci. Technol. 39 (06), 70–78. https://doi.org/10.13982/j.mfst.1673-9078.2023.6.0722.

Zhang, L., Yang, Y., Zhu, Y., Hu, H., Jia, Q., Sun, C., Zhu, X., Liu, Y., 2024. Antifungal activity and mechanism of chitosan against *Fusarium solani* caused ginger soft rot during postharvest storage. Postharvest Biol. Technol. 208, 112680. https://doi.org/10.1016/j.postharvbio.2023.112680.

Zhang, L., Zhang, B., Chen, S., Liu, M., Pan, W., Pu, Y., Hui, m, Xie, H., 2023. Inhibitory effect of endophytic antagonistic bacteria on two pathogenic fungi of *strawberry*. Jiangsu Agric. Sci. 51 (04), 121–127. https://doi.org/10.15889/j.issn.1002-1302.2023.04.018.

Zhang, X., Zhang, X., Li, H., Wang, S., Wang, Q., Li, S., 2019. Isolation and identification of lipopeptide antibiotic produced by *Bacillus amyloliquefaciens* B10-6-1 antagonistic to *Aspergillus flavus*. Mycosystema 38, 594–602. https://doi.org/10.13346/j.mycosystema.180296.

Zhong, L.Y., Zou, L., Tang, X.H., Li, W.F., Li, X., Zhao, G., Zhao, J.L., 2017. Community of endophytic fungi from the medicinal and edible plant *Fagopyrum tataricum* and their antimicrobial activity. Trop. J. Pharm. Res. 16 (2), 387–396. https://doi.org/10.4314/tjpr.v16i2.18.

Zhu, T., Yang, Z., 2000. A study on strain degeneration and its control of *Bacillus subtilis*. J. Southwest For. Coll. 01, 31–35.